



Climate variability, heat distribution, and polar amplification in the warm unipolar “icehouse” of the Oligocene

Dominique K. L. L. Jenny¹, Tammo Reichgelt², Charlotte L. O’Brien³, Xiaoqing Liu⁴, Peter K. Bijl¹, Matthew Huber⁴, and Appy Sluijs¹

¹Department of Earth Sciences, Utrecht University, 3584 CB Utrecht, the Netherlands

²Department of Earth Sciences, University of Connecticut, Storrs, CT 06269-1045, USA

³Department of Geography, University College London, WC1E 6BT, London, UK

⁴Department of Earth, Atmospheric, and Planetary Sciences, Purdue University, West Lafayette, IN 47907, USA

Correspondence: Dominique K. L. L. Jenny (d.k.l.l.jenny@uu.nl)

Received: 17 November 2023 – Discussion started: 4 December 2023

Revised: 16 April 2024 – Accepted: 16 May 2024 – Published: 25 July 2024

Abstract. The Oligocene (33.9–23.03 Ma) had warm climates with flattened meridional temperature gradients, while Antarctica retained a significant cryosphere. These may pose imperfect analogues to distant future climate states with unipolar icehouse conditions. Although local and regional climate and environmental reconstructions of Oligocene conditions are available, the community lacks synthesis of regional reconstructions. To provide a comprehensive overview of marine and terrestrial climate and environmental conditions in the Oligocene, and a reconstruction of trends through time, we review marine and terrestrial proxy records and compare these to numerical climate model simulations of the Oligocene. Results, based on the present relatively sparse data, suggest temperatures around the Equator that are similar to modern temperatures. Sea surface temperatures (SSTs) show patterns similar to land temperatures, with warm conditions at mid- and high latitudes ($\sim 60\text{--}90^\circ$), especially in the Southern Hemisphere (SH). Vegetation-based precipitation reconstructions of the Oligocene suggest regionally drier conditions compared to modern times around the Equator. When compared to proxy data, climate model simulations overestimate Oligocene precipitation in most areas, particularly the tropics. Temperatures around the mid- to high latitudes are generally underestimated in models compared to proxy data and tend to overestimate the warming in the tropics. In line with previous proxy-to-model comparisons, we find that models underestimate polar amplification and overestimate the Equator-to-pole temperature gradient suggested from the available proxy data. This further stresses the ur-

gency of solving this widely recorded problem for past warm climates, such as the Oligocene.

1 Introduction

Simulations of future climate change, by current-generation fully coupled climate models, indicate that global average surface warming will continue over the coming centuries depending on future CO₂ emissions and sequestration (IPCC, 2022). The models and available temperature, CO₂, and sea-level reconstructions of past Mesozoic and Cenozoic warm climates suggest that Earth’s climate may ultimately move towards unipolar conditions, with ice only remaining on Antarctica (Burke et al., 2018; Clark et al., 2016). Climate models additionally predict a global equilibrium surface warming between 1.5–4.5 °C per doubling of atmospheric CO₂ concentrations relative to pre-industrial values, most likely with a value around 3 °C (IPCC, 2022). This warming will be amplified at higher latitudes, notably the Arctic, by a factor of 2–3 relative to the global average (Fischer et al., 2018; Holland and Bitz, 2003; IPCC, 2022). However, model projections, particularly for such distant future non-analogue states, still include large uncertainties and are ideally independently constrained by data. Proxy-based reconstructions of past climates provide useful insights into the Earth’s natural response to CO₂ changes and are therefore an independent opportunity to quantify the sensitivity of various climate parameters to greenhouse forcing, including sea-

level and polar amplification (e.g., Burke et al., 2018; Lunt et al., 2016; Palaeosens Project Members, 2012). This way, climate models which are simulating past climate conditions can be compared against proxy data; hence the performance of the models can be evaluated.

It is likely that important climate parameters such as equilibrium climate sensitivity and polar amplification depend on the state of the climate (e.g., Farnsworth et al., 2019; Gaskell et al., 2022; Hutchinson et al., 2021; Köhler et al., 2015; Masson-Delmotte et al., 2013). Therefore, these parameters have been investigated for several past climate states. Traditional targets include the Pleistocene, Pliocene, and Eocene (e.g., Burke et al., 2018) and, more recently, the Miocene (Steinhorssdottir et al., 2021). These time intervals encompass a wide range of climate states, including those with ice sheets in both the Southern Hemisphere (SH) and Northern Hemisphere (NH), the Southern Hemisphere only, and ice-free states, in addition to a wide range of atmospheric greenhouse gas concentrations (e.g., Rae et al., 2021).

Recent work (e.g., O'Brien et al., 2020) has highlighted the Oligocene as a potentially useful climate state which allows us to assess the dynamics of global climate with only an Antarctic ice sheet present. Though geographical boundary conditions during the Oligocene (33.9–23.03 Ma – million years ago) were different to today, along with the Miocene, the Oligocene is a useful and relatively recent analogue to future unipolar icehouse climate states (e.g., O'Brien et al., 2020; Liebrand et al., 2017; Miller et al., 1988). Sparse, glacially deposited sediments suggest the presence of NH glaciers as young as the late Eocene (Eldrett et al., 2007; St. John, 2008), but there is no evidence for late Eocene large-scale continental glaciation. Instead, the cryosphere potentially comprised localised glaciers and restricted sea ice in the Arctic Ocean (DeConto et al., 2008; Stickley et al., 2009). Reconstructions of atmospheric CO₂ range from over 1000 ppm (parts per million) to as low as ~300 ppm for the Oligocene (Foster et al., 2017; Rae et al., 2021), similar to the range projected for the future based on various emission scenarios (IPCC, 2022). Despite potentially low atmospheric CO₂ conditions, the few available sea surface temperature (SST) reconstructions indicate temperatures warmer than modern climates throughout the Oligocene, with remarkable polar amplification (O'Brien et al., 2020).

Across the Eocene–Oligocene transition (EOT), atmospheric CO₂ concentrations dropped from >1000 ppm during the Eocene (56.0–33.9 Ma) to ~750 ppm or lower at the beginning of the Oligocene (Heureux and Rickaby, 2015; Paganini et al., 2005; Pearson et al., 2009). This drop coincides with a large increase (~1‰–1.5‰) in deep-ocean benthic foraminifer oxygen isotope ratios ($\delta^{18}\text{O}$), which includes the effects of both the formation of ice sheets and a drop in deep-sea temperatures (e.g., Coxall and Wilson, 2011). The forcings underlying the onset of the Oligocene so-called “icehouse” climate (i.e., with polar ice) are still highly debated. As of now, the leading hypothesis invokes a strongly non-

linear response to orbital forcing superimposed on a long-term drop in atmospheric CO₂ levels across a critical threshold (DeConto et al., 2008; DeConto and Pollard, 2003; Galeotti et al., 2016). However, the question that remains is if, or to what extent, tectonic changes and associated oceanographic reorganisations in the Southern Ocean (SO) played a role (e.g., Hill et al., 2013; Houben et al., 2019; Huber et al., 2004; Ladant et al., 2014; Sauermilch et al., 2021). Changes associated with the onset of polar glaciation include a drop in the global average temperature (Eldrett et al., 2009; Kotthoff et al., 2014; Liu et al., 2009; Meckler et al., 2022; Sluiter et al., 2022; Thompson et al., 2022; Zanazzi et al., 2007) and a profound change in deep-water temperatures (Meckler et al., 2022). Across the EOT, surface cooling (Liu et al., 2009), the accumulation of land ice that reached the Antarctic coastlines (Salamy and Zachos, 1999), and the consequent appearance of sea ice (Houben et al., 2013) were associated with pronounced changes in SH atmospheric circulation and oceanographic conditions (Diester-Haass and Zahn, 1996; Houben et al., 2019; Liu et al., 2009; Tripati et al., 2005) and an increase in the poleward ocean heat transport (Goldner et al., 2014). Global change at the beginning of the Oligocene also influenced the global turnover of flora and fauna (e.g., Solé et al., 2020; Sun et al., 2014). Oceanographic changes, including upwelling and the formation of sea ice, rapidly transformed circum-Antarctic marine ecosystems to such an extent that they may have influenced the evolution of large animal groups, such as the diversification amongst odontocete and mysticete (baleen) whales (e.g., Fordyce, 1980; Salamy and Zachos, 1999; Houben et al., 2013). Thus, the EOT seems to mark a prominent change in the global climate system (Westerhold et al., 2020) as continental ice sheets expanded.

Although the Oligocene has been the subject of numerous studies, the documentation of global Oligocene climate conditions and their variability, including the hemispheric distribution of heat, meridional temperature gradients, and biotic change, is sparse and greatly relies on benthic foraminifer isotope data. With the Earth's high-latitude cryosphere and climate directly responding to astronomical insolation changes, astronomical forcing studies of high-resolution benthic foraminifer $\delta^{18}\text{O}$ records are of great importance. Those studies (e.g., De Vleeschouwer et al., 2017; Galeotti et al., 2016; Levy et al., 2019; Liebrand et al., 2017; Naish et al., 2001; Pälike et al., 2006b) suggest significant variability in continental ice volume, paced by eccentricity and obliquity. Multiple-proxy SST data, albeit of much lower resolution than the deep-ocean $\delta^{18}\text{O}$ records, revealed that the Oligocene was characterised by generally warm climates, with flattened meridional temperature gradients (Gaskell et al., 2022; O'Brien et al., 2020). Still, Antarctica retained a significant cryosphere (e.g., Hoem et al., 2021). The recorded trends, cycles, and events provide ample opportunity to study the dynamics of climate and the carbon cycle in what has

been called a “doubthouse” or “intermediate” climate state (O’Brien et al., 2020).

In this paper, we aim to review the current state of knowledge regarding the Oligocene climate to provide a baseline for focused future research. To this end, we first provide basic constraints regarding important climatic boundary conditions, such as palaeogeography and atmospheric CO₂ levels. Additionally, a review of marine and terrestrial climate proxy records is presented, building on the compilation of marine records by O’Brien et al. (2020), to assess long-term trends and variability in the Oligocene climate. The temperature and precipitation data were subsequently compared to the results of two sets of Oligocene climate model simulations to evaluate how well we understand the data from a climate physics point of view. Lastly, we identify specific points of interest for follow-up research.

2 Oligocene stratigraphical and chronological framework

2.1 Oligocene chronostratigraphy

The Oligocene represents the epoch between two formal Global Stratotype Sections and Points (GSSPs), the Eocene–Oligocene boundary (EOB) and the Oligocene–Miocene boundary (OMB), at 33.9 and 23.04 Ma following GTS 2020 (Gradstein, 2020). The EOB GSSP was set in 1992 at the Massignano Quarry (Italy) and is defined by the extinction of the two planktic foraminifer genera *Hantkenina* and *Cribrohantkenina* at 33.9 Ma (Silva and Jenkins, 1993). The GSSP for the OMB was defined by Steininger et al. (1997) in the Tertiary Piedmont Basin in Italy on the magnetic reversal from polarity chron C6Cn.2r–C6Cn.2n between two subunits of the Rigoroso Formation. Later, Beddoe et al. (2018) dated the base of C6Cn.2n at 23.040 Ma. Within the Oligocene, Hardenbol and Berggren (1978) were the first to distinguish the Rupelian (33.9–27.29 Ma) from the Chattian (27.29–23.040 Ma) of northwestern Europe. They separated the two periods based on lithostratigraphy in Belgium into an open marine clayey unit which overlies a shallower marine sandy unit. The Rupelian (chron C13r–C9n) was introduced by Dumont (1849), describing the Boom Clay formation along the Rupel and Scheldt rivers in Belgium. The Chattian (chron C9n–C6Cn) was first officially mentioned by Fuchs (1894), who studied the “Kasseler Meeressande” (marine sands) in Hessen and Bünde, Germany (De Man et al., 2010; Van Simaeys, 2004; Van Simaeys et al., 2004). The GSSP for the Rupelian–Chattian boundary was set in 2016 by Coccioni et al. (2018) at the Monte Cagnero section near Urbania (Italy) and was bound by the (highest) last common occurrence (LCO) of the planktonic foraminifer *Chiloguembelina cubensis* at the base of the planktonic foraminifer zone O5. Currently, the official GSSP age for the Rupelian–Chattian boundary is 27.29 Ma, after Coccioni et al. (2018).

2.2 Oligocene isotope stratigraphy

Several informal definitions are used to describe the various stratigraphic isotope events associated with the Oligocene (Fig. 1). The Eocene–Oligocene transition (EOT) refers to the numerous climatic and environmental events broadly associated with the epoch boundary (e.g., Coxall and Pearson, 2007; Eldrett et al., 2009; Houben et al., 2012; Zanazzi et al., 2007). However, Hutchinson et al. (2021) recently defined it as the ~790 kyr interval between the extinction of the coccolithophore species *Discoaster saipanensis* (~34.46 Ma) and the Earliest Oligocene oxygen Isotope Step (EOIS). Hutchinson et al. (2021) also defined several other globally recognisable Oligocene isotope events, together replacing the classic Oligocene oxygen isotope zones of Miller et al. (1991). The EOIS, previously known as the onset of Oligocene oxygen isotope zone 1 (Oi-1; Miller et al., 1991), is an ~40 kyr long $\geq 0.7\text{\textperthousand}$ $\delta^{18}\text{O}$ increase (Coxall and Wilson, 2011; Zachos et al., 1996) which peaks at ~33.71 Ma. The EOT and the EOIS are followed by the Early Oligocene Glacial Maximum (EOGM), which lasted ~490 kyr from ~33.71 to ~33.22 Ma and chronostratigraphically correlates to most of the geomagnetic polarity timescale (GPTS) magnetostratigraphy C13n (33.726–33.214 Ma) (Hutchinson et al., 2021). The EOGM was first introduced by Liu et al. (2004) and spans the separate $\delta^{18}\text{O}$ maxima which were defined by Zachos et al. (1996) as Oi-1a (~33.66 Ma) and Oi-1b (~33.26 Ma), a consecutive period of colder climate and/or glaciation. The Mid-Oligocene Glacial Interval (MOGI) represents an ~1 Myr long phase of strong variability in $\delta^{18}\text{O}$ with marked maxima representing profound cooling and/or glacial expansion between 27.3 and 26.3 Ma (Liebrand et al., 2017), previously referred to as Oi-2b. The MOGI was followed by three warming phases (~26.3, ~25.5, and ~24.22 Ma), after which cooling led up to the Oligocene–Miocene transition (OMT; 23.88–23.04 Ma). The beginning of the Miocene (23.040–5.33 Ma) is marked by an ~1% rise in deep-ocean benthic foraminifer $\delta^{18}\text{O}$ values, traditionally referred to as the Mi-1 event (Billups et al., 2002; Flower et al., 1997; Miller et al., 1991).

3 Boundary conditions for Oligocene climate

3.1 Geographical boundary conditions

Oligocene plate tectonic geography differed from the modern configuration regarding several regions that are relevant to climate (Fig. 2). Specifically, plate tectonic movements may have been important for oceanographical change, influencing regional climate through changes in meridional and zonal heat transport. Here, we discuss the most prominent tectonic differences.

One of the most discussed tectonic changes since the Oligocene is the uplift of the Tibetan Plateau, the Himalayas, and the Hengduan Mountains. Although the collision be-

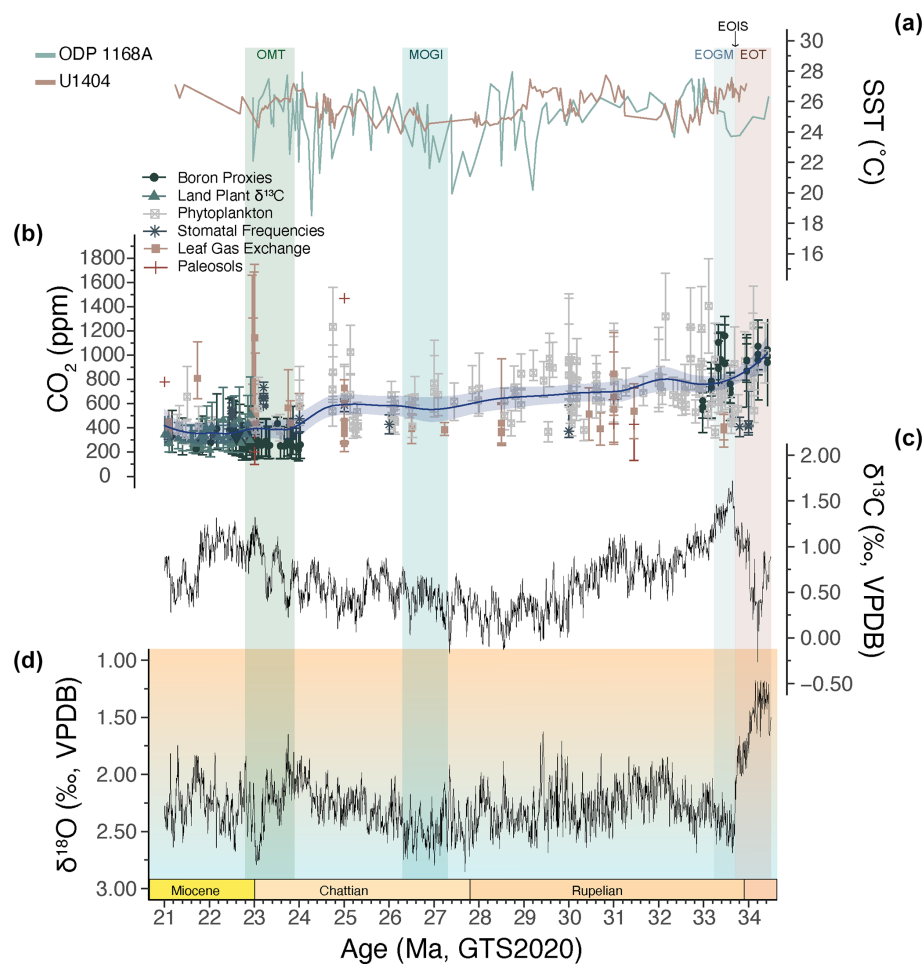


Figure 1. (a) In blue: SST of ODP 1168A (west of Tasmania, TEX^H₈₆; Guitián and Stoll, 2021; Hoem et al., 2021). In brown: SST of U1404 (northwestern Atlantic, UK37; Liu et al., 2018). (b) Published pCO₂ records of the Oligocene. Dark-blue line and shading represent the median and 95 % credible interval. Grey squares: phytoplankton data. Brown squares: leaf gas exchange reconstructions. Black dots: boron isotopic data. Green triangles: land plant $\delta^{13}\text{C}$ data. Brown crosses: palaeosol data. Green stars: stomatal frequency data (Greenop et al., 2019; Moraweck et al., 2019; Pagani et al., 2005, 2011; Roth-Nebelsick et al., 2014; Witkowski et al., 2018; Zhang et al., 2013; The CenCO2PIPm, 2023). (c, d) Deep-ocean benthic foraminifera stable carbon isotope and oxygen isotope records, respectively (Westerhold et al., 2020, notably representing the record of Pälike et al., 2006a). Red colour block: Eocene–Oligocene transition (EOT). Grey: Eocene–Oligocene Glacial Maximum (EOGM). Blue: Mid-Oligocene Glacial Interval (MOGI). Green: Oligocene–Miocene transition (OMT).

tween India and the Eurasian Plate predates the Oligocene (60–50 Ma; van Hinsbergen, 2022; Wang et al., 2014), continued collision also created further uplift of the Himalayas and the Tibetan Plateau in the Oligocene. The climatic consequences of the uplift are investigated both regionally (e.g., SE Asia; Ding et al., 2017; Su et al., 2019) and globally as a source of chemical weathering during the Cenozoic (e.g., Raymo and Ruddiman, 1992). Today, Tibet has an average elevation of over 4.5 km. During the Oligocene the elevation of Tibet was between 2.3 and 3 km, with central Tibet most likely at similar altitudes to today (Spicer et al., 2020, 2021a, b; Su et al., 2019).

Another important tectonic event during the Oligocene was the convergence of the European and Adriatic plates which led to the formation of the Alpine system. While

the collisional stage of the Alps began in the earliest Paleocene (65 Ma), during the Oligocene a slab from the subducted oceanic European lithosphere broke off, which resulted in the rapid and continued uplift of the Alps, which lasted until today but became stable in the mid-Miocene (Meschede and Warr, 2019). This resulted in an Oligocene uplift of ~ 1 km of the Alpine area, from an average elevation of < 1 to 2 km (Dielforder, 2017; Winterberg et al., 2020). Due to the strong tectonic changes around the eastern Alps and Tibet during the Oligocene, the so-called “Paratethys” (Laskarev, 1924), which reached from the western Molasse basin in Switzerland to the Aral Sea between Kazakhstan and Uzbekistan, became a semi-isolated inland sea at the beginning of the Oligocene (Schulz et al., 2005; Steininger and Wessely, 1999). The Paratethys consisted of a series of adj-

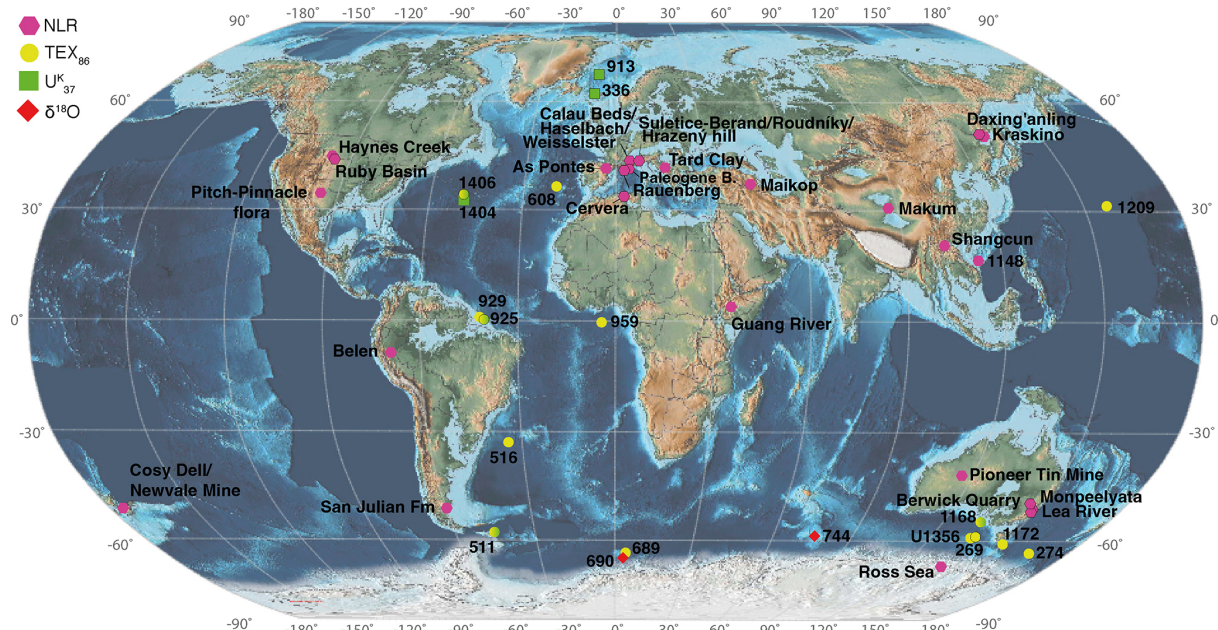


Figure 2. Palaeogeographic reconstruction of the Oligocene (~28 Ma). Yellow dots: Tex₈₆-based data. Purple hexagons: nearest living relative (NLR) data. Green squares: U₃₇^K data. Red diamonds: $\delta^{18}\text{O}$ data. Map created using GPlates, using the Scotese and Wright (2018) plate rotation.

cent sedimentary basins, of which the interconnections were rather unstable, resulting in the separation of the Paratethys into three main parts: the western (Alpine), central (Balkan), and eastern (Caucasian) Paratethys (Kováč, 2017; Palcu and Krijgsman, 2023; Rögl, 1998). A connection to the Mediterranean might have been established in the late Oligocene, connecting the Paratethys to the main oceans (Kováč, 2017).

Oceanic gateways in the Southern Ocean, including the Drake Passage (DP) and the Tasmanian Gateway, underwent tectonic changes in the Paleogene that were originally hypothesised to have strongly affected regional ocean circulation and associated heat and salt transport, as inferred from sedimentary data (e.g., Kennett, 1977; Murphy and Kennett, 1986). However, based on model simulations and biogeography, the extent to which the opening of these gateways affected Cenozoic cooling, either globally or regionally, remains the subject of debate (Houben et al., 2019; Huber et al., 2004; Kennett, 1977; Sauermilch et al., 2021; Scher and Martin, 2006; Toumoulin et al., 2020). While exact age estimates for the first opening of the DP lie most likely in the middle to late Eocene (~50 Ma; Eagles and Jokat, 2014), it remains likely that the DP opened once or experienced intermittent closures that resulted in staggered throughflow over several tens of millions of years (van de Lagemaat et al., 2021). The DP opened due to tectonic processes between the South American, Antarctic, and central Scotia plates (Eagles, 2016), and it involved a complex opening of isolated ocean basins which became oceanographically connected into one deep throughflow during the Oligocene (~26 Ma;

van de Lagemaat et al., 2021). During the early to middle Oligocene (34–26 Ma), subduction initiated between South America and the Scotia Plate (Crameri et al., 2020), which led to the opening and deepening of several ocean basins in the area between 29.5 and 21.2 Ma (van de Lagemaat et al., 2021). This tectonic development facilitated the formation of a deeper DP gateway (Maldonado et al., 2014).

Although spreading between Australia and Antarctica initiated in the Cretaceous, the South Tasman Rise connected the continents until the latest Eocene (see overview in Bijl et al., 2021). Dinoflagellate cyst biogeographical evidence suggests shallow-water connections between the Australo-Antarctic Gulf and the southwestern Pacific initiated close to the early–middle Eocene transition (Bijl et al., 2013). Lithological evidence for rapid deepening of the South Tasman Rise at ~35.7 Ma (Stickley et al., 2004) was later found to be a Southern Ocean-wide phenomenon related to the initiation of the throughflow of a vigorous Antarctic Counter Current and a proto-Antarctic Circumpolar Current (ACC; Houben et al., 2019). It is generally accepted that the Tasmanian Gateway was open to deep waters by Oligocene times (Stickley et al., 2004), but the Australian continent obstructed the optimal flow of strong circumpolar ocean currents until the late Neogene (Evangelinos et al., 2022; Hill et al., 2013; Sauermilch et al., 2021).

3.2 Ocean circulation

Using marine magnetic data, Barker and Burrell (1977) found that the opening of the Southern Ocean gate-

ways (SOGs) (i.e., the Drake Passage and the Tasmanian Gateway) preconditioned the formation of the Antarctic Circumpolar Current (ACC) between Antarctica, South America, and Australia. As Earth's strongest ocean current, the modern ACC is not only responsible for the regulation of heat and carbon exchange from and to the atmosphere, but it also influences deep-water formation and nutrient distribution (Cox, 1989; Scher et al., 2015). The ACC encircles Antarctica and, in doing so, connects the deep waters of the Pacific, Indian, and Atlantic oceans. Models using middle Eocene to early Oligocene geographies and CO₂ values have sought to understand the influence of the SOG openings on the global ocean (e.g., Goldner et al., 2014; Hutchinson et al., 2018; Kennedy et al., 2015; Kennedy-Asser et al., 2019; Sauermilch et al., 2021; Baatsen et al., 2016). Model simulations suggest that, as soon as the DP opened, a weak current (the proto-ACC) from the Pacific to the Atlantic would have been established (Ladant et al., 2014). Additionally, the coupled model of Toggweiler and Bjornsson (2000) shows that winds around Antarctica raise cold, dense water, cooling the region. This upwelled water then becomes fresher and warmer as it moves northwards due to Ekman transport. North of the ACC, this lighter and warmer water is transported downwards into the thermocline. This thickens the lower thermocline and creates a bigger density contrast across the Icelandic sills, ultimately enhancing the formation of North Atlantic Deep Water (NADW). Subsequently, NADW cools the water, facilitating its southward transport. The model of Toggweiler and Bjornsson (2000) shows that the DP opening thus might have led to a cooling of the air and oceans around Antarctica of around 3 °C. The water in the SH takes up the solar heat, which is then transported northwards where it is released, consequently warming up the NH by the equivalent amount the SH was cooled (Toggweiler and Bjornsson, 2000).

Lagabrielle et al. (2009) also discuss the influence of the proto-ACC on the formation and strength of Northern Component Water (NCW; later turns into NADW), which brings water from the NH to the Southern Ocean. Exactly when the formation of NCW began is unclear, but around 34 Ma the North Atlantic deepened rapidly due to its separation from Greenland in response to the Iceland mantle plume collapse, and significant deep-water production started in the NH (Lagabrielle et al., 2009; Via and Thomas, 2006). Hence, along with tectonic changes in the North Atlantic region, the proto-ACC contributed to the inception of NCW-/NADW and modulated its strength.

In the Eocene the SOGs were not open to deep-ocean circulation. Rather, shallow-ocean connections south of 60° S allowed a westward Antarctic Counter Current (e.g., Bijl et al., 2013; Houben et al., 2019). Although SOGs progressively opened in the Oligocene (Stickley et al., 2004), oceanographic changes associated with that were restricted to the Southern Ocean (Houben et al., 2019; Scher and Martin, 2008), and there was little effect on the Southern Ocean

oceanography for the remainder of the Oligocene (Evangelinos et al., 2020; Hill et al., 2013; Hoem et al., 2021; Wright et al., 2018). Only in the late Oligocene did Southern Ocean latitudinal SST gradients increase, and perhaps the ACC strengthened, due to deep opening of Drake Passage (Hoem et al., 2022), although the ACC weakened again during the Miocene Climatic Optimum (Evangelinos et al., 2022; Sangiorgi et al., 2018).

3.3 Atmospheric pCO₂

Only a few records of atmospheric pCO₂ cover the Oligocene entirely. Most are focused on the EOT and the OMT or are of low resolution. Trends are quite inconsistent between records and proxies (CenCO2PIP, 2023). The available records for the Oligocene are based on higher plant leaf gas exchange, phytoplankton ¹³C-fractionation, and foraminifer boron isotope ratios (Fig. 1). Pagani et al. (2005) were the first to produce a pCO₂ record for the Oligocene using ¹³C-fractionation of di-unsaturated alkenones extracted from various Deep Sea Drilling Project (DSDP) and Ocean Drilling Program (ODP) sediments. They recorded decreasing pCO₂ throughout the Oligocene from ~ 1500 ppm at the EOT to modern levels by the late Oligocene. Pagani et al. (2011) evaluated regional differences in pCO₂ and pCO₂ trends over the EOT by contrasting alkenone carbon isotope values from six DSDP and ODP sites. The estimated pCO₂ values yielded highly variable results among the different sites, showing a general atmospheric pCO₂ decline from around 1200 to around 600 ppm throughout the Oligocene, with pCO₂ decreasing around 40 % at the EOT. Zhang et al. (2013) critically evaluated confounding factors of the alkenone pCO₂ proxy and excluded data from several locations, arriving at a continuous CO₂ record covering the past 40 Ma based on di-unsaturated alkenone ¹³C-fractionation at ODP Site 925 in the western tropical Atlantic Ocean. The general findings of Zhang et al. (2013) agreed with the pCO₂ trends reported in Pagani et al. (2005, 2011) but showed pCO₂ values to decrease from ~ 1000 ppm at the EOT to ~ 400 ppm in the late Oligocene. Lastly, Witkowski et al. (2018) compiled the longest consecutive pCO₂ record of the past ~ 100 Ma, solely based on phytane ¹³C-fractionation from marine sediment and oil samples. Their results concur with the findings of Zhang et al. (2013), showing pCO₂ ranges from ~ 600–1000 ppm throughout the Oligocene with a decreasing trend from the EOT towards the OMT (Fig. 1). Both Roth-Nebelsick et al. (2014) and Morawec et al. (2019) used fossil leaf stomata to reconstruct Oligocene atmospheric pCO₂ levels. Oligocene fossil leaves of *Platanus neptuni* from various sites in Saxony (Germany) suggest lower pCO₂ levels than the alkenone-based results, with a modelled range of ~ 400–600 ppm for the Oligocene (Roth-Nebelsick et al., 2014). Morawec et al. (2019) reconstructed pCO₂ from the middle Eocene to the Oligocene using *P. neptuni* and *Rhodomyrtophyllum reticulosum* leaves

from seven central European sites. They found a similar $p\text{CO}_2$ range to Roth-Nebelsick et al. (2014), with values also varying between ~ 400 –600 ppm in the Oligocene. Greenop et al. (2019) created the only available boron-isotope-based $p\text{CO}_2$ record; however they only focus on the OMT. While Greenop et al. (2019) did not find a strong decreasing trend over the OMT, they generally found low, stable values ranging from around 220 to 350 ppm, which increased to around 400 ppm after the OMT.

While there is a lot of variability between Oligocene $p\text{CO}_2$ records, with plant and boron data showing relatively stable $p\text{CO}_2$ levels, most other records suggest a steady decline in atmospheric $p\text{CO}_2$ towards the Miocene (CenCO2PIP, 2023).

4 Climate proxy data

We compiled marine and terrestrial climate proxy data to assess long-term trends and variability in climate across the Oligocene. For sea surface temperatures, we have added recently published records to the compilation of O'Brien et al. (2020). To assess terrestrial climate, we compiled published records of fossil plant remains, notably pollen, spores, and macro-remains (Table A1). Where the fossil plant remains had been assigned taxonomic affinities, the nearest living relatives (NLRs) were determined and used as input for NLR-based probability density modelling, following the methodology of Willard et al. (2019) and Reichgelt et al. (2023), to assess terrestrial palaeoclimate. We adopt the age determination from the original sources (Table A1), corrected for the GTS 2020 stage boundaries (Gradstein, 2020), where, if absolute age determination is unavailable, an average age was taken. Based on the distribution of the NLR for each fossil species, the probability of plant co-existence in an assemblage is calculated for 60 000 combinations of mean annual temperature (MAT), winter mean temperature (WinT), mean annual precipitation (MAP), and driest-month precipitation (DMP), as plant species distributions are sensitive to these variables and significant differences exist in the analysed plant groups for these variables (see Supplement). Up to 20 different plant taxa were compared at a time, and, where there were more than 20 taxa, sets of 10 were randomly chosen to maximise data variability. We report the highest-probability climate combination, and the uncertainty range is based on those climatic combinations with a probability of $\geq 2.5\%$ of the maximum probability combination.

We found 28 vegetation reconstructions of sufficient quality to assess palaeoclimate using the NLR method (see Table A1). The results can be assigned several potential quality “flags” based on diversity, depositional environment, and taxonomical assignments. Firstly, low convergence of multiple simulations of the same flora may suggest that the climate niche of one or multiple taxa has changed since the

Oligocene (Reichgelt et al., 2023). Additionally, some floras had fewer than 20 taxa recorded, for which convergence could not be tested. Secondly, microfloras (pollen and spores) likely include upland or even extra-basinal input and are therefore less indicative of local climatic conditions than macrofloras (leaves, fruits, and flowers) (Reichgelt et al., 2023). Thirdly and finally, some palaeobotanical studies assign fossils to parataxa based on limited anatomical evidence or by using literature that is inappropriate for the study region. The majority of the data derives from NH mid-latitudes, a handful derives from SH mid-latitudes, and two datasets derive from the tropical realm. The absence of high-latitude data may be partly due to the lack of vegetation owing to cool conditions. However, there are pollen assemblages in sediments from the Antarctic margin (e.g., Askin and Raine, 2000; Prebble et al., 2005; Raine and Askin, 2001), but to our knowledge no quantitative data suitable for our NLR method have been generated for any high-latitude site.

4.1 Temperature

4.1.1 Continental mean annual temperature (MAT)

The data produced by the NLR allow a first assessment of the general Oligocene meridional temperature gradient on land. Unfortunately, the data are too sparse to assess trends or variability at any location, on any timescale (Fig. 3). Although the sparsity of data from low- and mid-latitude datasets limits our view on global gradients, the mid-latitude data can be compared to the modern and model simulations of the Oligocene and to reconstructed Eocene and Miocene gradients.

The two low-latitude data points suggest MATs of around $25\ ^\circ\text{C}$ ($\pm 1.5\ ^\circ\text{C}$). At first sight, Oligocene low-latitude MATs were, on average, similar to modern MATs for the same latitudes. However, the NLR method is based on modern distributions; therefore reconstructed temperatures cannot exceed the global temperature maximum. Palaeobotanical temperature reconstructions from the tropics are susceptible to this problem and should therefore be regarded as minimum estimates. Most mid-latitude MAT reconstructions in both the NH and SH are between 12 and $17\ ^\circ\text{C}$, with an average error of $\pm 2.9\ ^\circ\text{C}$ (Fig. 3). Mid-latitude MATs during the Oligocene, particularly in the SH, are generally higher (up to $16\ ^\circ\text{C}$) than modern temperatures. We did not encounter suitable data for high-latitude regions.

The reconstructed winter temperatures (WinTs) range from $\sim 23\ ^\circ\text{C}$ in the lower latitudes to $\sim 3\ ^\circ\text{C}$ in the highest-latitude samples ($\sim 52^\circ\text{N}$). Temperatures around the Equator reveal limited change in winter cooling ($\sim 1.8\ ^\circ\text{C}$), while at higher latitudes the difference in temperature between WinT and MAT can be up to nearly $8\ ^\circ\text{C}$. Compared to modern values, Oligocene WinTs show the same trend as MATs, with similar values (possibly underestimations) around the Equator and higher temperatures in the mid-latitudes (Fig. 3).

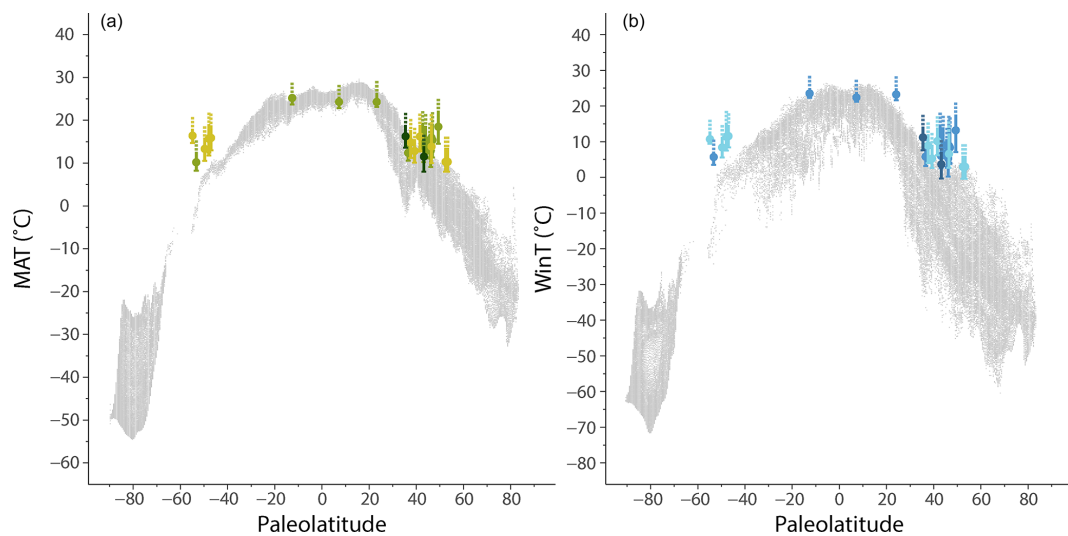


Figure 3. (a) Mean annual temperature (MAT; °C) plot over palaeolatitudes. In grey: pre-industrial (1900) MAT from Matsuura and Willmott (2018). (b) Winter temperature (WinT; °C) plot over palaeolatitudes. In grey: pre-industrial (1900) WinT from Matsuura and Willmott (2018). Darker colours represent a higher analytical certainty of the used site, and data with low reliability were excluded (see Table A1).

With the present dataset, it seems that Oligocene seasonality was similar to modern seasonality, with WinTs of the higher latitudes showing a difference of up to ~ 12 °C compared to the MATs, thus reflecting a high temperature change between MATs and WinTs. Just as in the modern period, Oligocene WinTs had a large range at higher latitudes, with temperatures varying between ~ 5 – 15 °C, whereas WinTs of lower latitudes barely show any temperature difference (Fig. 3).

4.1.2 Sea surface temperature

SSTs from three different proxies ($U_{37}^{k'}$, TEX₈₆, and biogenic calcite $\delta^{18}\text{O}$) were compiled for the low-, mid-, and high latitudes of the Oligocene (Fig. 4). The alkenone-based SST reconstruction ($U_{37}^{k'}$) relies on the temperature dependence of di- and tri-C₃₇ ketones (Prahl and Wakeham, 1987). At $U_{37}^{k'}$ values of > 0.9 (at SSTs > 27 °C) the proportion of the tri-unsaturated C₃₇ alkenone becomes very low, virtually absent and/or undetectable, setting an upper limit for the application of this proxy (Tierney and Tingley, 2018). In addition, the low proportion of this alkenone introduces analytical uncertainties that cause noise. Consequently, we regard all $U_{37}^{k'}$ values > 0.9 as representing SSTs at or above 27 °C. Following the recommendations by Hollis et al. (2019), we use the calibration of Müller et al. (1998; see Table A2).

The TEX₈₆ palaeothermometer is based on the temperature sensitivity of marine Thaumarchaeota membrane lipid (isoprenoid glycerol dialkyl glycerol tetraether (isoGDGT)) distributions (Schouten et al., 2002). The proportion of GDGTs containing a greater number of cyclopentane rings increases with higher temperatures and can thus be used to calculate SSTs using a modern surface sediment calibration (Wuchter et al., 2004). Discussion remains on how TEX₈₆

should be calibrated to represent seawater temperatures. The surface sediment calibration dataset shows virtually no response to temperatures below 15 °C, and it is debated if the response at the high-temperature end of the modern ocean – analogous to warmer climates in the past – can be assumed to be linear (e.g., O'Brien et al., 2017; Tierney and Tingley, 2014) or decreases exponentially (e.g., Cramwinckel et al., 2018; Kim et al., 2010). Moreover, isoGDGTs are barely produced in the mixed layer – they peak at ~ 50 – 200 m depth and sometimes somewhat deeper (e.g., Hurley et al., 2018; van der Weijst et al., 2022). Most calibrations include surface ocean temperatures in their calibration datasets, leading to an overestimation of the proxy slope (Ho and Laepple, 2016). As the Oligocene was most likely warmer than today, we therefore prefer a conservative approach to assess SST, using an exponential calibration that has a drop in proxy response at higher temperatures. Even though it is associated with regression dilution (Tierney and Tingley, 2014), we use the TEX₈₆^H of Kim et al. (2010; see Table A2) to assess SST, rather than a linear model, for reasons outlined in Fokkema et al. (2024). Linear models produce much higher SSTs in the Oligocene TEX₈₆ range (Hollis et al., 2019). Moreover, any SST calibration assumes a similar relationship between surface temperature and the isoGDGT export zone in both modern and ancient oceans. Given the above uncertainties, it should be noted that absolute TEX₈₆-derived SST estimates come with large uncertainties.

Planktic foraminifer oxygen isotope ratios were also used to estimate Oligocene SSTs. This method is based on the direct correlation between the temperature-dependent fractionation of the oxygen isotopes ^{16}O and ^{18}O into biogenic calcite of foraminifera (Shackleton, 1974). Here, the calibration of Kim and O'Neil (1997) is used because it is based on in-

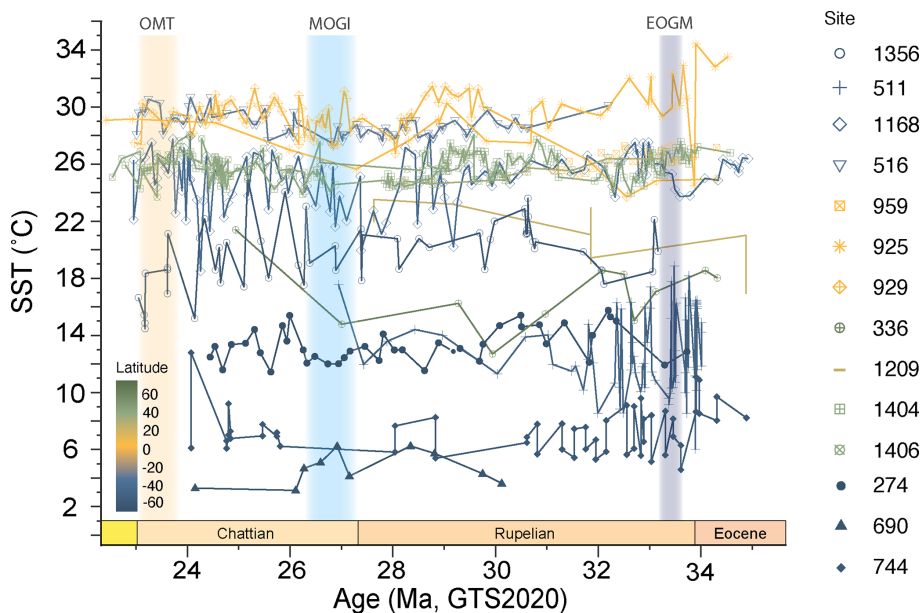


Figure 4. SST ($^{\circ}$ C) compilation for the Oligocene (CenCO2PIP, 2023). A linear interpolation was used between data points. Blue sites: SH high-latitude sites. Yellow sites: low-latitude sites. Green sites: NH high-latitude sites. See Fig. 2 for site locations and Table A3 for references.

organic calcite precipitated at temperatures between 10 and 40 $^{\circ}$ C and produces reliable results for foraminifera (Hollis et al., 2019). Foraminiferal calcite production has been found to decrease with increasing pH levels (Zeebe et al., 1999; Spero et al., 1997). The calibration of Kim and O’Neil (1997), may overestimate temperatures by up to 1.5 $^{\circ}$ C due to algal photosymbionts which modify the pH of the calcifying microenvironment (Spero and Williams, 1988). Although applying a direct correction is not recommended (Hollis et al., 2019) due to large uncertainties between symbiont activity levels, the influence of changing pH on SST reconstructions has to be considered.

Most available Oligocene SST data are from the mid-palaeolatitudes; records for the low- and high latitudes, especially in the NH, are scarce. Moreover, most records have low temporal resolution or cover only specific segments of the Oligocene (notably the EOT and OMT). The high latitude SSTs vary from 9.8 to 25.1 $^{\circ}$ C. It is worth noting that these records are restricted to latitudes no higher than 67° N and 68° S. SST estimates from mid-latitude locations have the largest temperature range, 6.0–32.1 $^{\circ}$ C, while SST estimates from low latitude sites span a narrower temperature range, 23.7–34.4 $^{\circ}$ C. The mid latitude SSTs show a slight increase (1–2 $^{\circ}$ C) between 34 and \sim 27 Ma, followed by a small decrease of 1–2 $^{\circ}$ C towards 23 Ma (Fig. 4). However, overall, there is a remarkable absence of long-term trends in these SST records.

To assess long-term changes in temperature and meridional temperature gradients, we analyse data from three time slices: 33.7–33.2, 27.3–26.3, and 23.9–23 Ma, corresponding

to the EOGM, MOGI, and OMT, which are averaged for an age of 33.4, 26.8, and 23.4 Ma, respectively. When SSTs are corrected for palaeolatitude (see Table A3), Oligocene SSTs are closer to late Eocene (\sim 38 Ma) than to modern values (Fig. 5). This is especially apparent in the Southern Ocean, where Oligocene SSTs are up to 10 $^{\circ}$ C warmer than modern SSTs. The high latitudes of the NH are challenging to assess due to data scarcity. However, the data available indicate that Oligocene SSTs were \sim 2 $^{\circ}$ C colder than Eocene SSTs but still \sim 4 $^{\circ}$ C warmer than modern SSTs. In contrast, low-latitude SST reconstructions show minimal differences, yielding similar temperature estimates for both the Oligocene and the Eocene. This leads to a flattened temperature gradient during the Oligocene between around 40° S and 40° N, where SSTs seem to be nearly the same.

4.2 Precipitation

Mean annual precipitation (MAP) and driest-month precipitation (DMP) were derived using the NLR approach (Table A1). The reconstructed MAP shows a range from \sim 850 to 1750 mm yr^{-1} . The SH mid-latitudes show a generally higher MAP (\sim 1200–1750 mm yr^{-1}) for the Oligocene compared to the NH (\sim 850–1650 mm yr^{-1}). This differs from modern MAP values, where there is not a big discrepancy between SH and NH MAP. Generally, the Oligocene MAP values are higher than modern values, especially at mid-latitudes. The few data points in the tropics suggest a MAP that is similar to modern MAP. The values for the driest month range from \sim 10 to 85 mm yr^{-1} , with generally lower

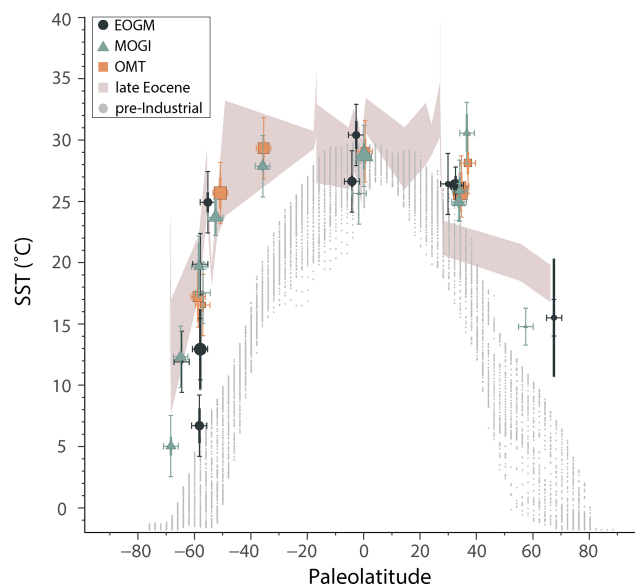


Figure 5. Sea surface temperatures (SSTs; $^{\circ}\text{C}$) over palaeolatitudes for 33.4 Ma (EOGM, black dots), 26.8 Ma (MOGI, blue triangles), and 23.4 Ma (OMT, orange squares). Brown shaded area: Baatsen et al. (2020) SST record for the late Eocene (38 Ma). Grey area: pre-industrial (1900) SST over latitude (Huang et al., 2015). Thick vertical error bars show the SST standard deviation, and thin vertical error bars represent the calibration error for each proxy. Larger symbols represent a higher data resolution, with larger symbols representing more data used and smaller points representing where fewer data were available. See Table A3 for data referral and references used.

values around the Equator and the NH ($\sim 10\text{--}45 \text{ mm yr}^{-1}$) and higher DMP in the SH ($\sim 20\text{--}85 \text{ mm yr}^{-1}$). The DMP values around the Equator are generally lower compared to modern values. In contrast to the Oligocene, the modern SH DMP values are on average lower than NH DMP values.

4.3 Data–model comparisons

The compiled surface temperature and precipitation data were regionally compared to the results from palaeoclimate model simulations (Figs. 7 and 8). Following the methodology described by O'Brien et al. (2020), two sets of modelling experiments were used: one from the NCAR Community Earth System Model version 1.0 (CESM1.0) and the other from the UK Hadley Centre Coupled Model version 3 (HadCM3L). The early and middle Oligocene simulations were performed using a $\times 3^{\circ}$ nominal ocean and the T31 atmospheric resolution with varying glaciation conditions and $p\text{CO}_2$ of 560 and 1120 ppm. The late Oligocene simulation used a $\times 1^{\circ}$ nominal ocean and 2° atmospheric resolution with a $p\text{CO}_2$ of 400 ppm. We compare data and simulations for three time slices: (a) early Oligocene, 33.9–33.0 Ma; (b) mid-Oligocene, 33.0–26.5 Ma; and (c) late Oligocene, 25.0–23.5 Ma (Fig. 7). For each time slice, the

model ensemble mean is used to compare with the data, and the modelling details of the ensemble members are found in the Methods and Supporting Information Table S1 of O'Brien et al. (2020). The model annual mean values are derived from the nearest grid point to the study site.

4.3.1 Temperature proxy–model comparison

Despite utilising two very distinct models with different boundary conditions, the temperature discrepancy between the model and data is similar. The comparison of sea and land temperatures of all three time slices show that the mid- and high-latitude proxy data generally suggest warmer local conditions than simulations predict (Fig. 7). For all investigated time slices, that discrepancy is largest in the North Atlantic and southwestern Pacific. Additionally, for every time slice, the tropics seem to be warmer in model simulations than what local proxy data find, with the most extreme discrepancies in continental southeastern Asia. For the early and middle Oligocene, there is a difference between the modelled higher latitudes and measured data. In both the early and middle Oligocene, the higher latitudes seem to be a lot warmer (up to 20°C) in the proxy data than what the models predict. The lower latitudes, on the other hand, for both the early and middle Oligocene, seem somewhat colder (around 5°C) than what models predict. In the early Oligocene, North America generally shows a similar temperature range to the European sites, with proxy data indicating warmer conditions compared to the model. This shifts in the middle Oligocene, where most of the recorded North American sites are colder than what the models predict. The late Oligocene seems to have a similar offset in the SH high latitudes, with reconstructed temperatures being up to nearly 20°C higher than the model results. Due to the lack of proxy data in the NH high latitudes and the tropics, temperature differences between models and records cannot be determined for the late Oligocene.

4.3.2 Precipitation proxy–model comparison

Comparison of precipitation proxy data to modelled simulations shows that, for all three simulated times, models mostly slightly underestimate the daily precipitation on a global scale (Fig. 8). In particular, the SH mid- to lower latitudes seem to be much drier in the models than what the proxy data suggest. For the early Oligocene, only NH tropical and NH mid-latitude data are available, indicating a slightly wetter ($300\text{--}400 \text{ mm yr}^{-1}$) climate in Europe, whereas eastern Asia and western North America appear to be drier ($300\text{--}900 \text{ mm yr}^{-1}$) than model predictions. Due to limited proxy data, we cannot make definitive statements about the early Oligocene in North America and eastern Asia. In the middle Oligocene, although more proxy data are available compared to the early Oligocene, the patterns are similar. Compared to the model results, the proxy data suggest wet-

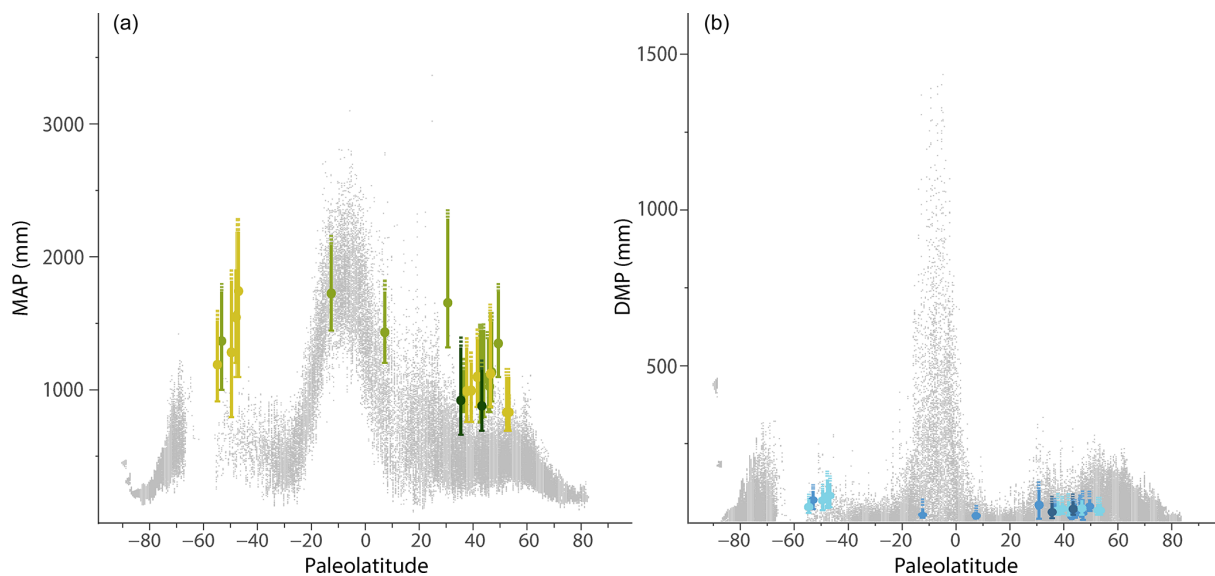


Figure 6. (a) Mean annual precipitation (MAP) plot over palaeolatitudes in mm yr^{-1} . In grey: pre-industrial (1900) MAP from Matsuura and Willmott (2018). (b) Driest-month precipitation (DMP) plot over palaeolatitudes in mm yr^{-1} . In grey: pre-industrial (1900) DMP from Matsuura and Willmott (2018). Darker colours represent a higher analytical certainty of the used site, and data with low reliability were excluded (see Table A1).

ter climates ($300\text{--}400 \text{ mm yr}^{-1}$) in Europe and eastern Asia ($600\text{--}900 \text{ mm yr}^{-1}$) and somewhat drier conditions ($300\text{--}900 \text{ mm yr}^{-1}$) in North America. In both the middle and late Oligocene, model simulations appear to underestimate precipitation in SH mid- to high latitudes ($300\text{--}900 \text{ mm yr}^{-1}$) (Fig. 8). Similarly to the early and mid-Oligocene, late Oligocene precipitation over central Europe and the region corresponding to today's Middle East also appears to be underestimated by models ($300\text{--}900 \text{ mm yr}^{-1}$), although precise quantifications cannot be made due to the lower proxy resolution.

5 Discussion

5.1 Temperature trends and variability

Not only does our compilation of data show that the Oligocene oceans were warm (O'Brien et al., 2020), but the sparsely available floral and faunal information from terrestrial settings shows pronounced warmth (Fig. 3). On average, the data indicate that the Oligocene was slightly cooler than the Eocene but much warmer than modern times (Figs. 3 and 5). Notably, the high latitudes were much warmer than in modern times. The current dataset suggests no or only modest tropical warming relative to the present, but it should be noted that this is based on few records and that the expected ocean warm pools have not yet been sampled. Both sea surface and terrestrial temperature gradients between the tropics and the SH midlatitudes were particularly small, which was previously recognised for the Eocene and for the Miocene (e.g., Baatsen et al., 2020; Burls et al., 2021; Hollis et al.,

2019; Lunt et al., 2021). For both Eocene and Oligocene SSTs, this is mainly the result of very high proxy values in the southwestern Pacific and the Australo-Antarctic Gulf (Baatsen et al., 2020; O'Brien et al., 2020). The gradient is very steep beyond 50°S (Fig. 5), while the Equator-to-pole temperature gradient in the NH is more gradual. This means that, despite the presence of ice in Antarctica, the mid-latitudes of the SH seem to be especially warm in the Oligocene.

Single-site high-resolution benthic foraminifer isotope data show a gradual decrease in $\delta^{18}\text{O}$ values across the late Oligocene up to the onset of the OMT (Fig. 1; De Vleeschouwer et al., 2017; Liebrand et al., 2016; Pälike et al., 2006b). This suggests pronounced warming during the late Oligocene, termed late Oligocene warming. Regionally, this warming is supported by biogeographical information (De Man and Simaeys, 2004). However, the compiled temperature records show no consistent evidence for long-term warming throughout the mid- to late Oligocene. Rather, they show relatively stable values, with only few records (e.g., ODP 925, 744) indicating cooling from the early to mid-Oligocene, followed by long-term warming from the mid- to late Oligocene (Fig. 4). This suggests that the decrease in $\delta^{18}\text{O}$ values may reflect regional warming at deep-water formation sites rather than global warming.

In the shorter term, there is strong variability within the temperature data, especially for the high and mid-latitudes (Fig. 4). Currently the resolution of all temperature records is insufficient to assess if any of this variability corresponds to orbital cyclicity. Similar variability apparent in deep-ocean

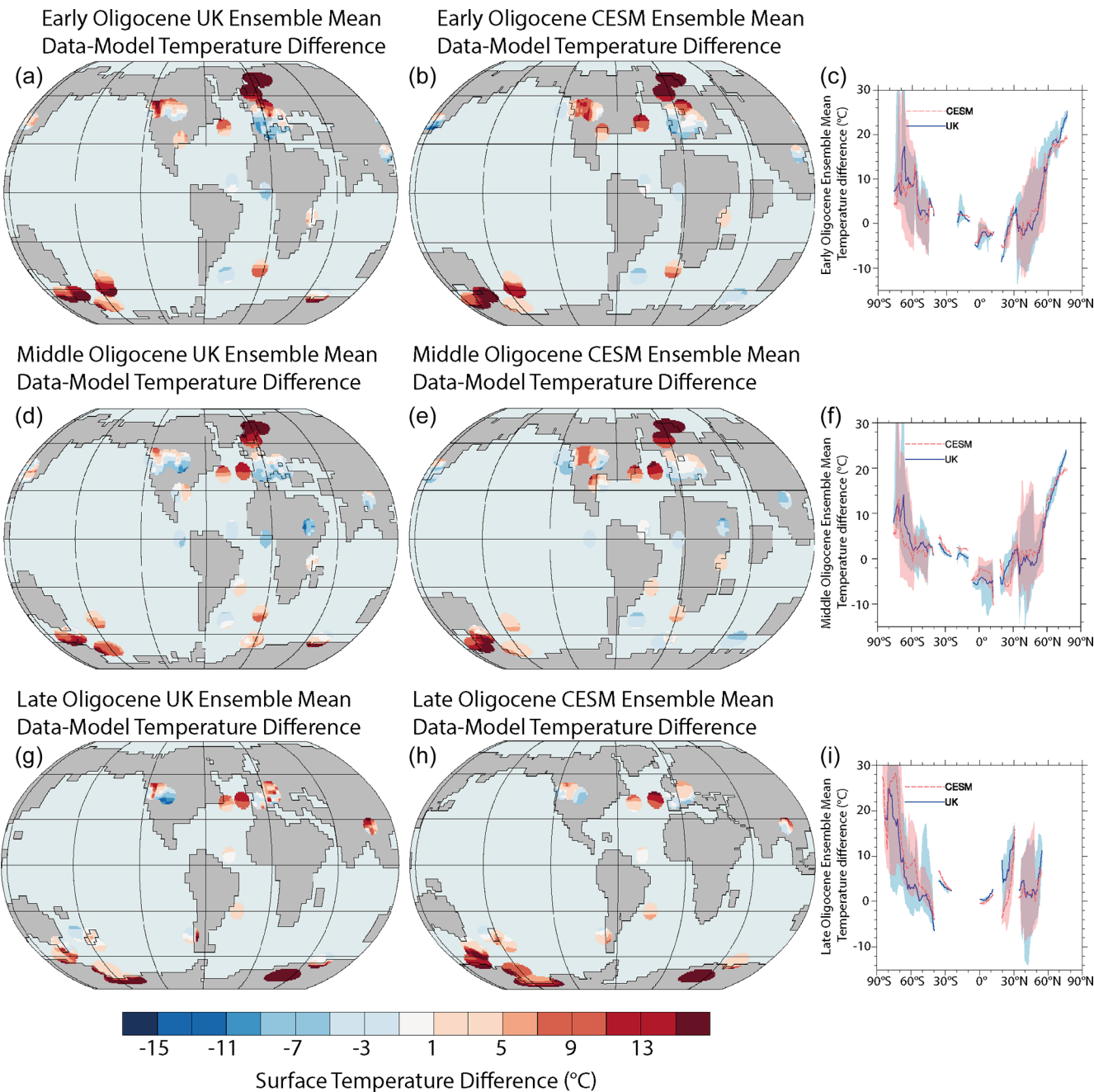


Figure 7. Oligocene temperature data–model comparisons. All proxy data were compared to ensemble means from HadCM3L (UK) and CESM. (a–i) Sea surface and land temperature data–model comparisons for three Oligocene time slices. Data–model temperature difference data are displayed both spatially (a, b, d, e, g, h) and as zonal means (c, f, i). Temperature difference data in panels (a), (b), (d), (e), (g), and (h) are calculated as pointwise differences between the proxy mean value and the model annual mean. The pink and blue ribbons in panels (c), (f), and (i) represent the maximum and minimum differences associated with the zonal means. All proxy data are shown in Table A4.

benthic $\delta^{18}\text{O}$ records primarily reflects eccentricity signals on timescales around 110 ka (Pälike et al., 2006b; Westerhold et al., 2020). If the temperature variability is global in nature, its increasing amplitude towards higher latitudes would likely reflect a combination of climatic polar amplification (i.e., ice and/or snow albedo and humidity feedbacks)

and/or oceanographic variability (i.e., fronts and upwelling). However, due to the low resolution and lack of temperature records, especially in low latitudes and in the NH, the nature of and mechanism behind the temperature variability remain uncertain.

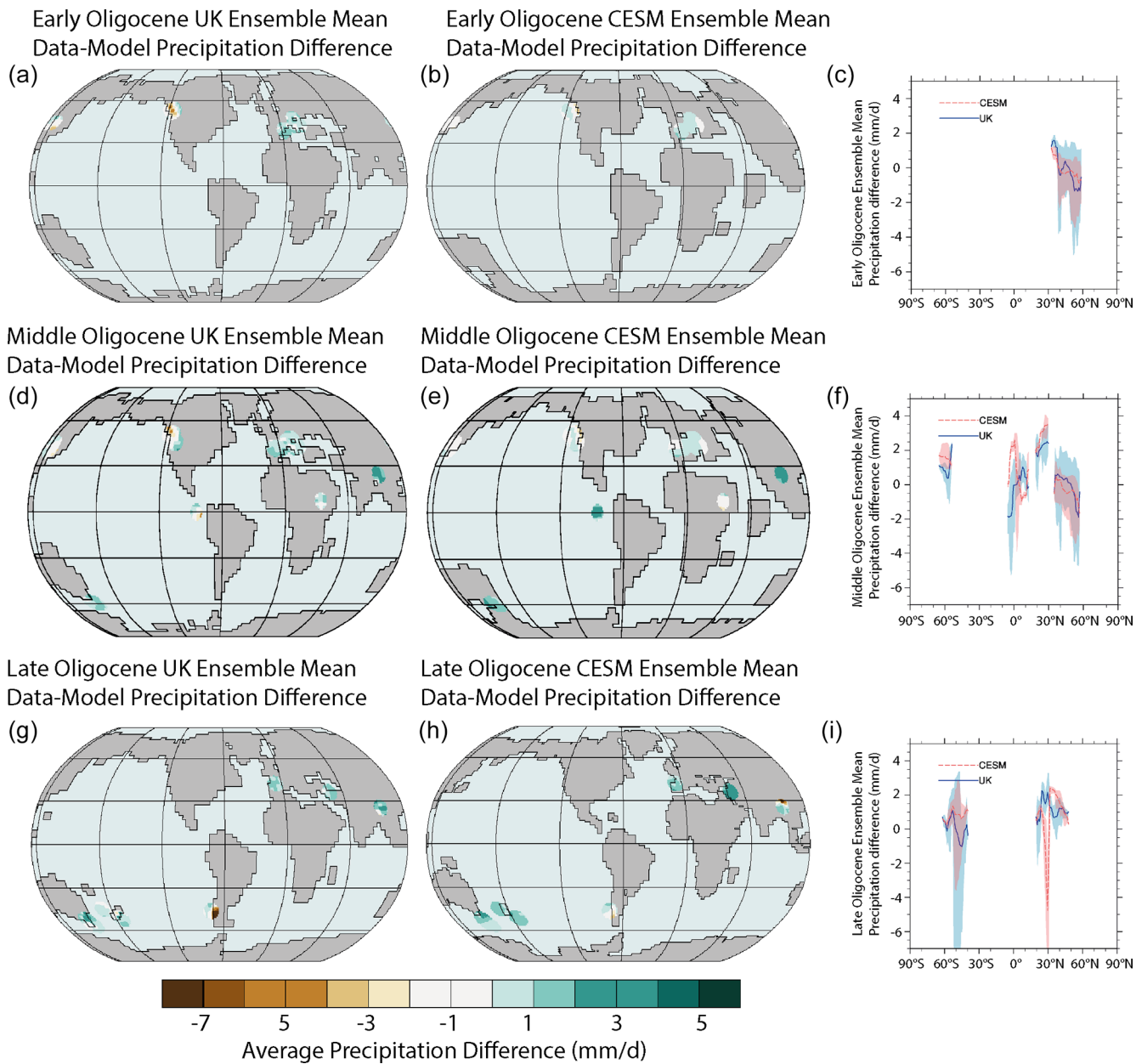


Figure 8. Oligocene precipitation data (mm d^{-1})–model comparisons. All proxy data were compared to ensemble means from HadCM3L (UK) and CESM. (a–i) Precipitation data–model comparisons for three Oligocene time slices. The data are displayed both spatially (a, b, d, e, g, h) and as zonal means (c, f, i) of the different precipitations. Differences in panels (a), (b), (d), (e), (g), and (h) are calculated as pointwise differences between the proxy mean value and the model annual mean and then plotted as points of difference. The pink and blue ribbons in panels (c), (f), and (i) represent the maximum and minimum differences associated with the zonal means. All proxy data are shown in Table A5.

When compared to model simulations (Figs. 7 and 8), it is evident that the models show significantly less polar amplification of warming relative to the present day than in the proxy data. This is due to the extremely strong warming at higher latitudes and comparatively modest warming in the tropics in the proxy data compared to the simulations. The dataset is limited, as floral data might underestimate tem-

peratures in tropical regions that are warmer than in modern times (e.g., Huber and Caballero, 2011). It should also be noted that some of the SST data are based on TEX₈₆, which suffers from large uncertainties in absolute SST reconstructions (see Sect. 4.1.2). However, plant-based (NLR) and U₃₇^{k'}-derived temperatures show similar warming to those based on TEX₈₆ in the high latitudes, corroborating strong

polar amplification. In other parts, climate models are not able to fully reconstruct regional climate variations as closely as proxy data can and thus probably underestimate regional variability, particularly on land (e.g., Laepple et al., 2023). Additional high-quality SST data are necessary to fully evaluate tropical temperatures for the Oligocene.

In particular, the shallow gradient between the Equator and $\sim 40^{\circ}$ N and S is difficult to reconcile with the simulations. Floral data and carbonate geochemical records support exceptional mid- to high-latitude warmth during the Eocene (e.g., Creech et al., 2010; Douglas et al., 2014; Willard et al., 2019), which still seems to be the case during the Oligocene. Collectively, the nature of the data might underestimate the latitudinal heat transfer for the Oligocene. Regardless, our findings agree with those of O'Brien et al. (2020), showing that most of the Oligocene was similar to the late Eocene greenhouse world. Like in the late Eocene (Baatsen et al., 2024), the recorded temperatures are difficult to reconcile with the formation and persistence of a large ice sheet on Antarctica. The model–data comparison highlights the ongoing challenges of fully understanding the complex nature of the Oligocene. Questions remain regarding the formation of ice in a world with a flattened meridional temperature gradient, when poles were much warmer than today and atmospheric CO₂ levels were high (e.g., Baatsen et al., 2020, 2024).

5.2 Precipitation

Surprisingly, the few MAP data points at low latitudes are similar to today (Fig. 6), whereas mid-latitude MAP is higher compared to pre-industrial values. DMP for the Oligocene low latitudes is especially low compared to the pre-industrial period. The Southern Hemisphere mid- to high-latitude DMP ($\sim 100 \text{ mm yr}^{-1}$) is higher than pre-industrial records ($< 100 \text{ mm yr}^{-1}$), whereas the DMP for the Northern Hemisphere is lower ($\sim 50 \text{ mm yr}^{-1}$), which is more in line with the pre-industrial records (0–250 mm yr⁻¹). During periods that are globally warmer than today, the tropics and the mid-latitudinal zone of converging westerlies ($30\text{--}60^{\circ}$ latitude) would be expected to be wetter than today, while the subtropics would be expected to be drier (e.g., Pierrehumbert et al., 2002). This is consistent with MAP reconstructions, especially at $> 30^{\circ}$ (Fig. 6a), whereas the data from lower latitudes are less clear, but that is largely due to a dearth of data points. Overall, Northern Hemisphere MAP is lower than that of the Southern Hemisphere. This may be due to the prevalence of Northern Hemisphere continental climate systems in the Oligocene (e.g., Sun et al., 2014). The Oligocene reconstructed MAP is somewhat lower than that of the Eocene (Cramwinckel et al., 2022). This drier climate compared to the Eocene is also seen in other terrestrial records (e.g., Couvreur et al., 2021; Dupont-Nivet et al., 2007; Jaramillo et al., 2006; Kohn et al., 2015; Ma et al., 2012; Salard-Cheboldaeff, 1979; Sun et al., 2014), which

suggests the expansion of arid regions and the reduction of rainforests during the Oligocene.

In addition, comparisons to modelled data show that the models underestimate, particularly in higher latitudes, precipitation levels from 300 up to over 900 mm yr⁻¹. Palaeoclimate models homogenise meso- and microclimates due to the large grid size, which leads to an averaged topography and thus less spatial precipitation variability. Proxy data, on the other hand, may experience a bias to wetter environments, as there is more plant data available where wetter climates persisted, including those in meso- or microclimates that were unrepresentative of the macroclimate, such as a riparian environment. Similar to temperature (Sect. 6.1), our understanding of global Oligocene precipitation relies on a limited dataset, mainly sampling Europe (Fig. 2); therefore a first-order goal to a more comprehensive understanding of Oligocene palaeoclimates would be to generate more terrestrial data from other continents, particularly from high-latitude regions.

6 Conclusions and outlook for future work

While the palaeogeography of the Oligocene differs from today, it still poses a useful analogue to a projected future unipolar climate state. It is becoming more and more clear that the Oligocene icehouse was in fact warmer than previously thought, particularly in mid- and high latitudes. However, the present dataset suggests that the tropical band was not much warmer than today. This is contrary to model simulations, which predict that tropical regions for the Oligocene were warmer than in modern times and are thereby most likely to underestimate polar amplification and subsequent Equator-to-pole heat distribution. From this perspective, the Oligocene also contrasts with reconstructions of tropical temperatures for the Miocene and Eocene (e.g., Steinthorsdottir et al., 2021; Hollis et al., 2019). Consequently, tropical climates during the Oligocene require further investigation in addition to the present dataset, which is notably based on biomarkers, so proxies based on well-preserved biogenic calcite derived from surface oceans are crucial. In contrast to tropical regions, proxy records at mid- and high-latitude regions suggest extreme warmth, as also noted for the Miocene and Eocene epochs (e.g., Steinthorsdottir et al., 2021; Hollis et al., 2019). The low temperature gradients indicated by our data remain a model–data mismatch that requires solving due to its implications for the processes governing polar amplification of greenhouse-gas-driven warming and the magnitude thereof.

The limited vegetation data available support higher precipitation in mid-latitude regions during the Oligocene, as predicted by theory and model simulations. However, the continental dataset is limited, and more data are required particularly for the tropical band and the high latitudes to test for

tropical hydrology and high-latitude winter temperatures, respectively.

Our temperature compilation does not show systematic long-term changes in temperature during the Oligocene. With the typically low resolution of the available long-term records, temperatures remained approximately stable. This is at odds with the long-term trends in the benthic foraminifera $\delta^{18}\text{O}$ record, which shows signs of early Oligocene cooling and late Oligocene warming, albeit low in magnitude. Higher-resolution SST reconstructions at multiple locations are required to fully evaluate if those trends are absent on Earth's surface. Moreover, the apparent absence of long-term trends in SST and the nature of the minor trends in benthic foraminifera $\delta^{18}\text{O}$ are both inconsistent with the recorded long-term drop in atmospheric $p\text{CO}_2$. This is a truly interesting conundrum and one that requires long-term high resolution $p\text{CO}_2$ reconstructions to fully evaluate. Although the benthic foraminifera $\delta^{18}\text{O}$ records have identified the orbital-scale dynamics of deep-ocean temperature and/or continental ice volume in detail, orbital-scale climate variability of the Oligocene on the surface is poorly constrained. SST records resolving orbital-scale variability are required to ultimately characterise the nature of global mean surface temperature variability and the magnitude of polar amplification, its dependence on atmospheric $p\text{CO}_2$, and its relation to global continental ice volume.

Finally, an outstanding question remains on the relation of climate variability and subsequent biotic change. There is ample micropalaeontological evidence for a biotic response to orbital-scale temperature variability for the Oligocene (e.g., De Man and Simaeys, 2004; Śliwińska et al., 2010; Hoem et al., 2021; Fenero et al., 2013). The interplay of long-term climate stability and superimposed orbital-scale variability provides a very interesting opportunity to investigate the systematic relation between such climate variability and biotic resilience. This requires long-term, high-resolution micropalaeontological records but might ultimately result in much better-defined thresholds of massive regime shifts.

Appendix A

Table A1. Results of the nearest living relative (NLR) analysis, showing mean annual temperature (MAT), winter mean temperatures (WinT), mean annual precipitation (MAP), driest-month precipitation (DMP), and their respective minimum and maximum values.

Locality	Average age (Ma)	Latitude	Palaeolatitude	Number of taxa	Number of quality flags	Number of simulations	Min MAT (°C)	Max MAT (°C)	Min WinT (°C)	Max WinT (°C)	Min MinT (°C)	Max MinT (°C)	Min MAP (mm yr ⁻¹)	Max MAP (mm yr ⁻¹)	Min DMP (mm yr ⁻¹)	Max DMP (mm yr ⁻¹)	Max References				
As Ponte basin	26.1 ± 3.7	43.45	37.62	14	1	Taxa assignments dubious, one simulation, macrofloras	11.2	14.8	17.7	4.0	8.9	12.1	-0.8	1.9	7.0	759	1000	1318	20	38	63 Calvera et al. (1995)
Baile fruit and seed assembly	29.25 ± 0.75	-4.75	-12.62	17	1	Taxa assignments reliable, one simulation, macrofloras	23.7	25.2	25.9	22.3	23.5	25.0	15.1	16.9	18.9	1445	1738	2089	11	20	40 Manchester et al. (2012)
Berwick Quarry	25	-38.03	-47.02	33	10	Taxa assignments reliable, high convergence, macro and microfloras	13.0	15.9	18.8	8.4	11.6	14.7	3.5	6.1	9.5	1096	1754	2188	44	78	120 Pole et al. (1993)
Calau Beds	29.5 ± 1.5	51.78	46.86	56	10	Taxa assignments reliable, medium convergence, macrofloras	11.3	15.4	19.2	3.9	8.4	13.7	-1.3	2.6	6.5	912	1143	1514	4	24	69 Mai (1998)
Cerro de Raqui quarry, Cañua quarry, Mus Claret, Briançó	30.85 ± 3.05	41.65	35.44	28	10	Taxa assignments reliable, high convergence, macroflora	13.6	16.3	18.9	7.6	11.2	14.2	1.7	5.5	8.8	661	955	1318	9	24	58 Tosi and Martin-Closas (2016)
Cosy Dell	24.9 ± 0.5	-46.15	-47.91	65	10	Taxa assignments reliable, medium convergence, microfloras	12.6	15.8	17.8	8.6	11.4	14.0	3.5	6.2	8.9	1202	1556	1905	48	74	115 Comman et al. (2014)
Daxing	31.15 ± 2.75	45.86	52.40	24	10	Taxa assignments reliable, high convergence, microfloras	8	10.3	13.6	-0.4	3.0	6.0	-5.3	-1.5	1.5	692	843	1096	20	32	55 Ma et al. (2012)
Daxing, uniting 2	31.31	46.31	53.31																		
Guang River	27.23	12.60	7.24	19	1	Taxa assignments reliable, one simulation, macrofloras	22.8	24.3	25.5	21.2	22.4	23.9	14.3	16.9	18.4	1202	1445	1738	24.3	14	29 Pan (2007)
Hasselt horizon	29.75 ± 0.75	51.42	46.45	32	10	Taxa assignments reliable, medium convergence, macroflora	12.8	15.9	18.8	4.9	8.9	13.9	-0.2	3.3	7.5	871	1143	1585	15.9	33	55 Kunzmann and Walther (2012)
Haynes Creek Flora	30	45.00	43.22	29	10	Taxa assignments reliable, high convergence, microfloras	8	11.5	13.9	-0.3	3.7	7.1	-5.4	-0.7	2.4	692	891	1148	11.5	37	63 Axeldorff (1998)
Hrazený hill	29.5 ± 1.5	50.98	46.11	32	10	Taxa assignments reliable, low convergence, microfloras	9.1	12.9	16.2	0.2	5.4	9.0	-5.8	0.9	3.2	832	1038	1380	12.9	35	66 Kváček et al. (2015)
Krasikov Flora	30	42.71	49.33	31	10	Taxa assignments reliable, low convergence, microfloras	14.5	18.5	22.2	7.1	13.2	17.6	1.9	6.4	11.4	1096	1361	1738	18.5	43	69 Pavlyukin (2011)
River Lea	31 ± 1	-41.50	-53.28	10	1	Taxa assignments reliable, one convergence, microfloras	8.2	10.2	12.6	3.5	5.7	7.2	-0	1.3	3.5	1000	1380	1738	10.2	63	95 Pauli and Hill (2010)
Makun Group	25	40.55	39.29	30	10	Taxa assignments reliable, high convergence, microfloras	10.1	12.8	15.6	2.6	5.3	9.1	-1.9	0.8	3.3	759	1005	1202	12.8	36	58 Popov et al. (2008)
Makun Coal Field	26.2 ± 3.2	27.25	25.46	23	10	Taxa assignments dubious, high convergence, microfloras	23.1	24.3	26.4	21.6	23.2	24.9	16.4	18.5	20.7	1318	1667	2291	24.3	45	100 Awasthi and Mehrotra (1995)
Monpelyatia deposit	23.3 ± 0.9	-41.83	-49.68	43	10	Taxa assignments reliable, medium convergence, microfloras	10.5	13.3	15.9	5.6	8.4	11.3	0.2	3.2	6.5	794	1294	1820	13.3	63	100 Macphail et al. (1991)
New Vale Mine	24.1 ± 1.1	-46.14	-47.91	99	10	Taxa assignments reliable, low convergence, microfloras	11.8	15.7	19.1	7.5	11.4	15.3	2.5	6.3	10.9	1096	1556	2188	15.7	84	132 Ferguson et al. (2010)
Paleogene basin	30.45 ± 3.45	46.35	41.54	26	10	Taxa assignments reliable, low convergence, microfloras	12.8	16.2	18.9	6.2	10.2	13.9	1.1	4.0	7.6	871	1107	1380	16.2	38	63 Erdéi et al. (2012)
Pitch-Pinnacle flora	30.95 ± 1.95	39.12	36.56	17	1	Taxa assignments reliable, one simulation, macrofloras	10.6	12.4	13.9	3.2	5.8	7.8	-1.4	0.8	2.4	832	1047	1148	12.4	38	52 Gregory and Mclintosh (1996)
Raueberg	29.5 ± 2.5	49.27	43.97	35	10	Taxa assignments reliable, medium convergence, microflora	12.3	15.3	18.7	5.6	9.0	14.0	0.9	4.1	8.1	794	1091	1445	15.3	30	55 Kovář-Eder (2016)
Roudnicky area	31.95 ± 1.95	50.65	45.75	33	10	Taxa assignments reliable, medium convergence, microfloras	11.2	14.1	16.8	2.8	6.9	10.6	-2.6	1.7	4.7	832	1102	1380	14.1	35	58 Kváček et al. (2014)
San Julian Fin	24	-49.16	-54.85	18	1	Taxa assignments reliable, one simulation, macrofloras	14.7	16.4	18	9.4	10.7	12.8	2.5	4.1	6.9	912	1202	1514	16.4	42	69 Palazzi and Barreda (2007)
Sulejów-Bernard	27.5 ± 1.5	50.61	45.89	17	1	Taxa assignments reliable, one simulation, microflora	12.6	14.5	16.1	6.0	8.7	10.3	0.5	1.8	4.4	871	1096	1380	14.5	42	60 Kváček and Walther (1995)
Tard Clay 1	32.9 ± 0.9	47.50	42.73	12	1	Taxa assignments reliable, one simulation, macroflora	14.6	16.9	19.4	8.3	11.6	14.8	2.5	7.0	8.9	759	1000	1445	8	13	35 Kváček et al. (2001)
Upper Ruby Basin	32.9 ± 0.7	45.11	43.10	65	10	Taxa assignments reliable, medium convergence, macroflora	10.2	13.5	16.8	2.7	6.0	11.0	-2.8	1.3	5.4	794	1028	1318	18	34	58 Becker (1966)
Weischester Basin	29.75 ± 0.75	51.42	46.45	79	10	Taxa assignments reliable, low convergence, macrofloras	10.0	13.9	18.9	2.7	6.6	12.3	-1.7	1.5	5.7	871	1138	1585	20	39	66 Gastaldo et al. (1998)

Table A2. Summary of the calibrations and references thereof used for the respective sea surface temperature (SST) proxies.

SST proxy	SST calibration details	References
U_{37}^K	U_{37}^K' indices were converted to SST estimates using the global core-top calibration of Müller et al. (1998).	Müller et al. (1998)
TEX ₈₆	TEX ₈₆ values were converted to SST using the global logarithmic TEX ₈₆ ^H calibration of Kim et al. (2010)	Kim et al. (2010)
Δ_{47}	Δ_{47} SST estimates and sample age were taken directly from the original publications.	Douglas et al. (2014), Petersen and Schrag (2015) Evans et al. (2018), Briard et al. (2020)
$\delta^{18}\text{O}$ coccoliths	SST estimates are original published values for small coccoliths with a vital effect correction in Tremblin et al. (2016).	Tremblin et al. (2016)
$\delta^{18}\text{O}$ planktic foraminifera	Palaeotemperature estimates were generated using the calibration of Kim and O'Neil (1997).	Kim and O'Neil (1997)

Table A3. Summary of all compiled sea surface temperatures (SSTs) for all site locations including the analytical and calibration errors used for each proxy. Top: available SST data for the Oligocene Miocene Transition (OMT). Middle: available SST data for the Mid-Oligocene Glacial Interval (MOGI). Bottom: available SST data for the Eocene Oligocene Glacial Maximum (EOGM).

Site	Latitude	Longitude	Event	Average age (Ma)	Proxy	Number of data points	Palaeolatitude	Lowest latitude	Highest latitude	Min latitudinal error	Max latitudinal error	Average SST ($^{\circ}$ C)	Standard deviation ($^{\circ}$ C)	Analytical error ($^{\circ}$ C)	Calibration error ($^{\circ}$ C)	References
23.9–24.0 Ma																
269	-61.68	140.07	OMT	23.4	TEX ₈₆	2	-57.1	-59.73	-54.53	2.7	2.5	16.54	0.54	1.00	2.50	Evangelinos et al. (2020)
1356	-63.31	136.00	OMT	23.4	TEX ₈₆	9	-58.7	-61.38	-56.18	2.6	2.6	17.23	2.04	1.00	2.50	Hartman et al. (2018)
1168	-42.61	144.41	OMT	23.4	TEX ₈₆ , U ₃₇ ^K	14	-50.9	-53.54	-48.33	2.7	2.5	25.68	1.29	1.00	2.50	Guitian and Stoll (2021), Hoem et al. (2022)
1404	40.01	-51.81	OMT	23.4	U ₃₇ ^K	18	34.2	31.69	36.89	2.5	2.7	25.70	0.58	0.30	1.50	Liu et al. (2018)
1406	40.35	-51.65	OMT	23.4	U ₃₇ ^K , TEX ₈₆	7	34.5	32.01	37.22	2.5	2.7	26.21	1.17	1.00	2.50	Guitian et al. (2019)
608	42.84	-23.09	OMT	23.4	TEX ₈₆	4	36.9	34.38	39.59	2.5	2.7	28.14	0.93	1.00	2.50	Super et al. (2020)
929	5.98	-43.74	OMT	23.4	TEX ₈₆	5	0.4	-2.16	3.05	2.6	2.6	29.08	1.00	1.00	2.50	O'Brien et al. (2020), Liu et al. (2009)
516	-30.28	-35.29	OMT	23.4	TEX ₈₆	10	-35.5	-38.20	-33.00	2.7	2.5	29.33	0.77	1.00	2.50	O'Brien et al. (2020)
27.3–28.3 Ma																
336	63.35	-7.79	MOGI	26.8	U ₃₇ ^K	1	57.4	54.81	60.01	2.5	2.7	14.77	0.00	0.30	1.50	Liu et al. (2009)
511	-51.00	-46.97	MOGI	26.8	TEX ₈₆	1	-57.0	-59.67	-54.47	2.7	2.5	17.54	0.00	1.00	2.50	Liu et al. (2009), Houben et al. (2019)
516	-30.28	-35.29	MOGI	26.8	TEX ₈₆	6	-35.8	-38.51	-33.31	2.7	2.5	27.87	0.41	1.00	2.50	O'Brien et al. (2020)
274	-69.00	173.43	MOGI	26.8	TEX ₈₆	6	-64.9	-67.57	-62.37	2.6	2.6	12.31	0.33	1.00	2.50	Hoem et al. (2021)
1356	-63.31	136.00	MOGI	26.8	TEX ₈₆	5	-58.5	-61.14	-55.94	2.6	2.6	19.68	1.89	1.00	2.50	Hartman et al. (2018)
1168	-42.61	144.41	MOGI	26.8	U ₃₇ ^K	9	-52.6	-55.23	-50.03	2.7	2.5	23.69	1.44	0.30	1.50	Guitian and Stoll (2021), Hoem et al. (2022)
1404	40.01	-51.81	MOGI	26.8	TEX ₈₆	8	33.7	31.15	36.36	2.5	2.7	24.95	0.48	0.30	1.50	Liu et al. (2018)
925	4.20	-43.49	MOGI	26.8	TEX ₈₆	1	-1.7	-4.36	0.85	2.6	2.6	25.64	0.00	1.00	2.50	Liu et al. (2009), Zhang et al. (2013), Ingels et al. (2015), Cramwinckel et al. (2018)
1406	40.35	-51.65	MOGI	26.8	U ₃₇ ^K , TEX ₈₆	4	34.0	31.48	36.68	2.5	2.7	25.86	1.15	1.00	2.50	Guitian et al. (2019)
929	5.98	-43.74	MOGI	26.8	TEX ₈₆	17	0.0	-2.59	2.62	2.6	2.6	28.72	1.08	1.00	2.50	O'Brien et al. (2020), Liu et al. (2009)
608	42.84	-23.09	MOGI	26.8	TEX ₈₆	2	36.5	33.97	39.18	2.5	2.7	30.57	1.52	1.00	2.50	Super et al. (2020)
690	-65.16	1.20	MOGI	26.8	$\delta^{18}\text{O}$	4	-68.4	-71.06	-65.86	2.6	2.6	5.03	0.77	1.00	2.50	Ehrmann and Mackensen (1992), Gaskell et al. (2022)
33.7–33.8 Ma																
274	-69.00	173.43	EOGM	33.4	TEX ₈₆	1	-64.6	-67.31	-61.91	2.7	2.7	11.91	0.00	1.00	2.50	Hoem et al. (2021)
511	-51.00	-46.97	EOGM	33.4	U ₃₇ ^K , TEX ₈₆	13	-58.0	-60.77	-55.36	2.8	2.6	12.94	3.29	1.00	2.50	Liu et al. (2009), Plancton et al. (2014), Houben et al. (2019)
913	75.49	6.95	EOGM	33.4	U ₃₇ ^K	2	67.4	64.76	70.17	2.7	2.7	15.51	4.80	0.30	1.50	Liu et al. (2009)
1356	-63.31	136.00	EOGM	33.4	TEX ₈₆	1	-58.0	-60.74	-55.34	2.8	2.6	19.87	0.00	1.00	2.50	Hartman et al. (2018)
1168	-42.61	144.41	EOGM	33.4	TEX ₈₆	5	-55.3	-58.07	-52.67	2.8	2.6	24.92	0.83	1.00	2.50	Hoem et al. (2022)
1404	40.01	-51.81	EOGM	33.4	U ₃₇ ^K	13	32.5	29.90	35.31	2.6	2.8	26.30	0.78	0.30	1.50	Liu et al. (2018)
1209	32.65	158.51	EOGM	33.4	TEX ₈₆	2	29.8	27.20	32.61	2.6	2.8	26.42	0.06	1.00	2.50	Kast et al. (2019)
959	3.63	-2.74	EOGM	33.4	TEX ₈₆	6	-4.2	-6.95	-1.54	2.7	2.7	26.63	0.46	1.00	2.50	Cramwinckel et al. (2018)
925	4.20	-43.49	EOGM	33.4	TEX ₈₆ , $\delta^{18}\text{O}$	4	-2.7	-5.45	-0.03	2.7	2.7	30.41	1.13	1.00	2.50	Liu et al. (2009), Zhang et al. (2013), Ingels et al. (2015), Cramwinckel et al. (2018), Tremblin et al. (2016)
744	-61.58	80.60	EOGM	33.4	$\delta^{18}\text{O}$	6	-58.3	-61.08	-55.67	2.8	2.6	6.70	1.41	1.00	2.50	Barron et al. (1991), Gaskell et al. (2022)

Table A4. All sea surface temperature (SST) data per site location that were added to the O'Brien et al. (2020) data–model comparison, including standard deviations and lower quartile (LQ) and upper quartile (UQ) errors. Top: all available SST data between 33.9–33 Ma. Middle: all available SST data between 22–26.5 Ma. Bottom: all available SST data between 25–23 Ma.

Site	Age (Ma)	Palaeolatitude (33 Ma)	Palaeolongitude (33 Ma)	Proxy	Error (°C)	Mean (°C)	Median (°C)	Lower quartile (°C)	Upper quartile (°C)	LQ incl. error (°C)		UQ incl. error (°C)		True value	True value incl. error			
33.9–33 Ma																		
Cervera	33.9–27.8	38.44	2.43	NLR	1.8	16.3	16.1	14.5	12.7	18.0	19.7	13.6	18.9	11.8	20.7	Tosal and Martín-Closas (2016)		
Daxing'anling	33.4–28.4	43.73	120.42	NLR	2.3	10.3	10.3	8.7	6.3	13.2	15.5	8.0	13.6	5.7	15.9	Ma et al. (2012)		
IODP168A	34.9–22.9	-62.90	149.63	TEX86	0.9	25.4	25.6	25.0	24.1	26.0	26.9	23.7	26.4	22.8	27.3	Hoem et al. (2022)		
ODP 274	33.7–24.5	-70.24	177.16	TEX86	0.7	12.4	12.4	12.1	11.4	12.6	13.3	11.9	12.8	11.3	13.5	Hoem et al. (2021)		
ODP 744	34.9–24.1	-63.68	75.30	$\delta^{18}\text{O}$	1.9	7.9	8.2	6.6	4.7	8.7	10.6	4.6	11.1	2.7	13.0	Barren and Huber (1991), Gaskell et al. (2022)		
33–26.5 Ma																		
Paleogene basin	33.9–27.0	42.08	14.10	NLR	1.6	16.2	16.1	14.2	12.6	17.5	19.1	12.8	18.9	11.2	20.5	Erdei et al. (2012)		
Roudnicky area	33.9–30.0	46.27	15.68	NLR	1.8	14.1	14.4	12.6	10.8	16.2	18.0	11.2	16.8	9.4	18.6	Kváček and Walther (1995)		
Tard Clay	33.8–32.0	42.71	19.85	NLR	2.4	16.9	16.9	14.6	12.2	19.4	21.8	14.6	19.4	12.2	21.8	Kváček et al. (2001)		
Upper Ruby Basin	33.6–32.2	51.56	-115.06	NLR	1.7	13.5	13.3	11.6	9.9	15.0	16.7	10.2	16.8	8.5	18.5	Becker (1966)		
As Pontes basin	29.8–22.4	41.37	-61.13	NLR	3.3	14.8	14.8	11.2	7.9	17.7	21.0	11.2	17.7	7.9	21.0	Cabrera et al. (1995)		
Belén fruit and seed assemblage	30.0–28.5	0.05	-84.71	NLR	1.1	25.2	25.2	23.7	22.6	25.9	27.0	23.7	25.9	22.6	27.0	Manchester et al. (2012)		
Calau Beds	31.0–28.0	47.80	15.65	NLR	1.8	15.4	15.6	13.3	11.5	16.8	18.6	11.3	19.2	9.5	21.0	Ferguson et al. (2010)		
Cervera	33.9–27.8	41.65	1.33	NLR	1.8	16.3	16.1	14.5	12.7	18.0	19.7	13.6	18.9	11.8	20.7	Tosal and Martín-Closas (2016)		
Daxing'anling	33.9–28.4	44.03	121.21	NLR	2.3	10.3	10.3	8.7	6.3	13.2	15.5	8.0	13.6	5.7	15.9	Ma et al. (2012)		
Guang River	27.23	7.31	34.03	NLR	1.4	24.3	24.3	22.8	21.4	25.5	26.9	22.8	25.5	21.4	26.9	Pan (2007)		
Haselbach horizon	30.5–29.0	47.48	14.95	NLR	1.5	15.9	15.6	14.1	12.6	17.1	18.7	12.8	18.8	11.3	20.3	Kunzmann and Walther (2012)		
Haynes Creek Flora	30.0	50.89	-116.83	NLR	1.9	11.5	11.4	9.6	7.7	13.3	15.2	8.0	13.9	6.1	15.8	Axeldrof (1998)		
Hrazený hill	31.0–28.0	46.94	16.09	NLR	1.9	12.9	13.2	11.7	9.8	15.3	17.2	9.1	16.2	7.2	18.1	Kváček et al. (2015)		
IODP168A	34.9–22.9	-60.95	148.67	TEX86	1.4	25.3	25.4	24.6	23.3	26.4	27.7	21.9	27.9	20.5	29.3	Hoem et al. (2022)		
IODP168A	29.2–22.9	-60.95	148.67	$^{\text{U}}\text{K}_{37}$	1.5	21.3	21.1	20.4	18.9	22.1	23.6	19.2	23.4	17.7	24.9	Gutiérrez and Stoll (2021)		
Krasikino Flora	30.0	40.09	122.70	NLR	1.6	18.5	18.8	16.9	15.3	20.2	21.9	14.5	22.2	12.9	23.8	Pavlyukin (2011)		
River Lea	32.0–30.0	-59.66	149.94	NLR	2.2	10.2	10.2	8.2	6.0	12.6	14.8	8.2	12.6	6.0	14.8	Paul and Hill (2010)		
Makum Coal Field	29.4–23.0	24.42	92.74	NLR	1.2	24.3	23.9	23.5	22.3	25.8	27.0	23.1	26.4	21.9	27.6	Awasthi and Mehrotra (1995)		
ODP 274	33.7–24.5	-70.03	176.95	TEX86	1.2	13.5	13.3	12.5	11.3	14.6	15.8	11.4	15.7	10.2	17.0	Hoem et al. (2021)		
ODP 690	30.1–24.2	-64.25	-5.70	$\delta^{18}\text{O}$	1.2	4.6	4.5	3.7	2.6	5.6	6.7	3.1	6.2	2.0	7.4	Mackensen and Ehrmann (1992), Gaskell et al. (2022)		
ODP744	34.9–24.1	-63.58	75.92	$\delta^{18}\text{O}$	1.2	7.0	6.9	6.0	4.8	7.8	8.9	5.3	9.6	4.1	10.8	Barren and Huber (1991), Gaskell et al. (2022)		
Paleogene basin	33.9–27.0	42.44	14.05	NLR	1.6	16.2	16.1	14.2	12.6	17.5	19.1	12.8	18.9	11.2	20.5	Erdei et al. (2012)		
Pitch-Pinnacle flora	32.9–29.0	44.93	-108.88	NLR	1.7	12.4	12.4	10.6	8.9	13.9	15.6	10.6	13.9	8.9	15.6	Gregory and McIntosh (1996)		
Rauenberg	32.0–27.0	45.68	10.51	NLR	1.8	15.3	15.1	13.6	11.8	17.2	19.0	12.3	18.7	10.5	20.5	Mai (1998)		
Roudnicky area	33.9–30.0	46.65	15.57	NLR	1.8	14.1	14.4	12.6	10.8	16.2	18.0	11.2	16.8	9.4	18.6	Kváček and Walther (1995)		

Table A4. Continued.

Site	Age (Ma)	Palaeolatitude (33 Ma)	Palaeolongitude (33 Ma)	Proxy	Error (°C)	Mean (°C)	Median (°C)	Lower quartile (°C)	Upper quartile (°C)	LQ incl. error (°C)	UQ incl. error (°C)	True value		True value incl. error		
												Min value (°C)	Max value (°C)	Min value (°C)	Max value (°C)	Reference
Sulejice-Berand	29.0–26.0	46.59	15.82	NLR	1.8	14.5	14.5	12.6	10.8	16.1	17.9	12.6	16.1	10.8	17.9	Cabréa et al. (1995)
Tard Clay	33.8–32.0	43.17	19.82	NLR	2.4	16.9	16.9	14.6	12.2	19.4	21.8	14.6	19.4	12.2	21.8	Kváček et al. (2001)
Upper Ruby Basin	33.6–32.2	50.98	-114.80	NLR	1.7	13.5	13.3	11.6	9.9	15.0	16.7	10.2	16.8	8.5	18.5	Becker (1966)
Weisselstier	30.5–29.0	47.48	14.95	NLR	1.7	13.9	13.5	12.4	10.7	15.6	17.3	10.0	18.9	8.3	20.6	Gastaldo et al. (1998)
<i>25–23 Ma</i>																
As Pontes basin	29.8–22.4	41.80	-6.44	NLR	3.3	14.8	14.8	11.2	7.9	17.7	21.0	11.2	17.7	7.9	21.0	Cabréa et al. (1995)
Berwick Quarry	25.0	-52.34	147.39	NLR	1.2	15.9	15.6	14.5	13.3	16.7	17.9	13.0	18.8	11.8	20.0	Gastaldo et al. (1998)
Cosy Dell	25.4–24.4	-44.80	170.69	NLR	1.3	15.8	15.7	14.3	13.0	16.8	18.1	12.6	17.8	11.3	19.1	Connan et al. (2014)
IODP1168A	34.9–22.9	-57.00	147.14	TEX ₈₆	2.3	24.6	25.2	23.0	20.7	26.4	28.7	18.5	27.9	16.2	30.3	Hoern et al. (2022)
IODP1168A	29.2–22.9	-57.00	147.14	U ₃₇ ^K	1.7	25.3	25.7	24.2	22.5	26.3	28.0	22.6	28.1	20.9	29.8	Gutiérrez and Stoll (2021)
Maikop Group	25.0	35.96	47.13	NLR	1.7	12.8	12.8	10.9	9.2	14.2	15.9	10.1	15.6	8.4	17.3	Popov et al. (2008)
Makum Coal Field	29.4–23.0	25.46	93.70	NLR	1.2	24.3	23.9	23.5	22.3	25.8	27.0	23.1	26.4	21.9	27.6	Awasthi and Mehrotra (1995)
Monpelyata deposit	24.2–22.4	-55.94	149.71	NLR	1.9	13.3	13.3	11.1	9.1	14.9	16.8	10.5	15.9	8.6	17.8	Macphail et al. (1991)
New Yale Mine	25.2–23.0	-51.28	-174.24	NLR	1.3	15.7	15.9	14.4	13.1	17.0	18.4	11.8	19.1	10.5	20.4	Connan et al. (2014)
ODP274	33.7–24.5	-69.65	176.37	TEX ₈₆	0.8	12.7	12.8	12.2	11.4	13.2	14.1	11.6	13.3	10.8	14.2	Hoern et al. (2021)
ODP744	34.9–24.1	-63.36	77.13	$\delta^{18}\text{O}$	3.3	7.9	6.3	6.1	2.8	8.1	11.4	6.1	12.8	2.8	16.0	Barreira and Huber (1991), Gaskell et al. (2022)
San Julian Fm	24.0	-45.93	-74.05	NLR	1.7	16.4	16.4	14.7	13.0	18.0	19.7	14.7	18.0	13.0	19.7	Palazzi and Barreda (2007)

Code availability. All scripts and programs can be accessed at <https://doi.org/10.5281/zenodo.10144091> (Jenny et al., 2023a).

Data availability. All supplementary data are available at <https://doi.org/10.5281/zenodo.10143889> (Jenny et al., 2023b).

Supplement. The supplement related to this article is available online at: <https://doi.org/10.5194/cp-20-1627-2024-supplement>.

Author contributions. DKLLJ made the data compilation with CLO. The scripts and programs for the precipitation model were written by XL, and the scripts and programs for the sea surface temperature data were written by MH. TR ran the nearest living analysis on compiled fossil plant remains. DKLLJ wrote the article with PKB and AS with contributions from all authors.

Competing interests. At least one of the (co-)authors is a member of the editorial board of *Climate of the Past*. The peer-review process was guided by an independent editor, and the authors also have no other competing interests to declare.

Disclaimer. Publisher's note: Copernicus Publications remains neutral with regard to jurisdictional claims made in the text, published maps, institutional affiliations, or any other geographical representation in this paper. While Copernicus Publications makes every effort to include appropriate place names, the final responsibility lies with the authors.

Acknowledgements. We thank the editor, the reviewers, and a colleague who contacted us informally for their constructive feedback on our paper.

Financial support. This work was carried out under the programme of the Netherlands Earth System Science Centre (NESSC); has been financially supported by the Ministry of Education, Culture, and Science (OCW) through Gravitation (grant no. 024.002.001); and has received funding from the European Union's Horizon 2020 research and innovation programme under the Marie Skłodowska-Curie Actions (grant no. 847504). Appy Sluijs has also been funded through support from the European Research Council Consolidator (grant no. 71497).

Review statement. This paper was edited by Gerilyn (Lynn) Soreghan and reviewed by two anonymous referees.

References

- Askin, R. A. and Raine, J. I.: Oligocene and Early Miocene Terrestrial Palynology of the Cape Roberts Drillhole CRP-2/2A, Victoria Land Basin, Antarctica, *Terra Antartica*, 7, 493–501, 2000.
- Awasthi, N. and Mehrotra, R.: Oligocene flora from Makum Coalfield, Assam, India|*Journal of Palaeosciences, Palaeobotanist*, 44, 157–188, 1995.
- Axelrod, D. I.: The Oligocene Haynes Creek Flora of Eastern Idaho, University of California Press, 164 pp., ISBN 9780520098244, 1998.
- Baatsen, M., van Hinsbergen, D. J. J., von der Heydt, A. S., Dijkstra, H. A., Sluijs, A., Abels, H. A., and Bijl, P. K.: Reconstructing geographical boundary conditions for palaeoclimate modelling during the Cenozoic, *Clim. Past*, 12, 1635–1644, <https://doi.org/10.5194/cp-12-1635-2016>, 2016.
- Baatsen, M., von der Heydt, A. S., Huber, M., Kliphuis, M. A., Bijl, P. K., Sluijs, A., and Dijkstra, H. A.: The middle to late Eocene greenhouse climate modelled using the CESM 1.0.5, *Clim. Past*, 16, 2573–2597, <https://doi.org/10.5194/cp-16-2573-2020>, 2020.
- Baatsen, M., Bijl, P., von der Heydt, A., Sluijs, A., and Dijkstra, H.: Resilient Antarctic monsoonal climate prevented ice growth during the Eocene, *Clim. Past*, 20, 77–90, <https://doi.org/10.5194/cp-20-77-2024>, 2024.
- Barker, P. F. and Burrell, J.: The opening of Drake Passage, *Mar. Geol.*, 25, 15–34, [https://doi.org/10.1016/0025-3227\(77\)90045-7](https://doi.org/10.1016/0025-3227(77)90045-7), 1977.
- Barrera, E. C. and Huber, B. T.: Paleogene and early Neogene oceanography of the southern Indian Ocean: Leg 119 foraminifer stable isotope results, in: Proceedings of the Ocean Drilling Program, Scientific Results, edited by: Barron, J., Larsen, B., Anderson, J., and Baldauf, J. Q., Ocean Drilling Program, College Station, TX, 693–717, <https://doi.org/10.2973/odp.proc.sr.119.167.1991>, 1991.
- Barron, J. A., Baldauf, J. G., Barrera, E., Caulet, J. P., Huber, B. T., Keating, B. T., Lazarus, D., Sakai, H., Thierstein, H. R., and Wei, W.: Biochronologic and magnetostratigraphic synthesis of Leg 119 sediments from the Kerguelen Plateau and Prydz Bay, Antarctica, *Proc. ODP, Sci. Results*, 119, 813–847, <https://doi.org/10.2973/odp.proc.sr.119.188.1991>, 1991.
- Becker, H. F.: Additions to and Revision of the Oligocene Ruby Paper Shale Flora of Southwestern Montana, *Contrib. Museum Paleontol.*, 20, 89–119, 1966.
- Beddow, H. M., Liebrand, D., Wilson, D. S., Hilgen, F. J., Sluijs, A., Wade, B. S., and Lourens, L. J.: Astronomical tunings of the Oligocene-Miocene transition from Pacific Ocean Site U1334 and implications for the carbon cycle, *Clim. Past*, 14, 255–270, <https://doi.org/10.5194/cp-14-255-2018>, 2018.
- Bijl, P. K., Bendle, J. A. P., Bohaty, S. M., Pross, J., Schouten, S., Tauxe, L., Stickley, C. E., McKay, R. M., Röhl, U., Olney, M., Sluijs, A., Escutia, C., and Brinkhuis, H.: Eocene cooling linked to early flow across the Tasmanian Gateway, *P. Natl. Acad. Sci. USA*, 110, 9645–9650, <https://doi.org/10.1073/pnas.1220872110>, 2013.
- Bijl, P. K., Frieling, J., Cramwinckel, M. J., Boschman, C., Sluijs, A., and Peterse, F.: Maastrichtian–Rupelian paleoclimates in the southwest Pacific – a critical re-evaluation of biomarker paleothermometry and dinoflagellate cyst paleoecol-

- ogy at Ocean Drilling Program Site 1172, *Clim. Past*, 17, 2393–2425, <https://doi.org/10.5194/cp-17-2393-2021>, 2021.
- Billups, K., Channell, J. E. T., and Zachos, J.: Late Oligocene to early Miocene geochronology and paleoceanography from the subantarctic South Atlantic, *Paleoceanography*, 17, 4-1–4-11, <https://doi.org/10.1029/2000PA000568>, 2002.
- Briard, J., Pucéat, E., Vennin, E., Daëron, M., Chavagnac, V., Jaillet, R., Merle, D., and de Rafélis, M.: Seawater paleotemperature and paleosalinity evolution in neritic environments of the Mediterranean margin: Insights from isotope analysis of bivalve shells, *Palaeogeogr. Palaeoclim. Palaeoecol.*, 543, 109582, <https://doi.org/10.1016/j.palaeo.2019.109582>, 2020.
- Burke, K. D., Williams, J. W., Chandler, M. A., Haywood, A. M., Lunt, D. J., and Otto-Bliesner, B. L.: Pliocene and Eocene provide best analogs for near-future climates, *P. Natl. Acad. Sci. USA*, 115, 13288–13293, <https://doi.org/10.1073/pnas.1809600115>, 2018.
- Burls, N. J., Bradshaw, C. D., De Boer, A. M., Herold, N., Huber, M., Pound, M. J., Donnadieu, Y., Farnsworth, A., Frigola, A., Gasson, E., Von Der Heydt, A. S., Hutchinson, D. K., Knorr, G., Lawrence, K. T., Lear, C. H., Li, X., Lohmann, G., Lunt, D. J., Marzocchi, A., Prange, M., Riihimaki, C. A., Sarr, A. C., Siler, N., and Zhang, Z.: Simulating Miocene Warmth: Insights From an Opportunistic Multi-Model Ensemble (MioMIP1), *Paleoceanogr. Paleoclim.*, 36, 40, <https://doi.org/10.1029/2020PA004054>, 2021.
- Cabrera, L., Hagemann, H. W., Pickel, W., and Sáez, A.: The coal-bearing, Cenozoic As Pontes basin (northwestern Spain): geological influence on coal characteristics, *Int. J. Coal Geol.*, 27, 201–226, [https://doi.org/10.1016/0166-5162\(94\)00021-Q](https://doi.org/10.1016/0166-5162(94)00021-Q), 1995.
- CenCO2PIP – The Cenozoic CO₂ Proxy Integration Project Consortium: Toward a Cenozoic history of atmospheric CO₂, *Science*, 382, eadi5177, <https://doi.org/10.1126/science.adl5177>, 2023.
- Clark, P. U., Shakun, J. D., Marcott, S. A., Mix, A. C., Eby, M., Kulp, S., Levermann, A., Milne, G. A., Pfister, P. L., Santer, B. D., Schrag, D. P., Solomon, S., Stocker, T. F., Strauss, B. H., Weaver, A. J., Winkelmann, R., Archer, D., Bard, E., Goldner, A., Lambeck, K., Pierrehumbert, R. T., and Plattner, G.-K.: Consequences of twenty-first-century policy for multi-millennial climate and sea-level change, *Nat. Clim. Change*, 6, 360–369, <https://doi.org/10.1038/nclimate2923>, 2016.
- Coccioni, R., Montanari, A., Bice, D., Brinkhuis, H., Deino, A., Frontalini, F., Lirer, F., Maiorano, P., Monechi, S., Pross, J., Rochette, P., Sagnotti, L., Sideri, M., Sprovieri, M., Tateo, F., Touchard, Y., Simaeys, S. V., and Williams, G. L.: The Global Stratotype Section and Point (GSSP) for the base of the Chattian Stage (Paleogene System, Oligocene Series) at Monte Cagnero, Italy, *Episodes*, 41, 17–32, <https://doi.org/10.18814/epiugs/2018/v41i1/018003>, 2018.
- Conran, J. G., Mildenhall, D. C., Lee, D. E., Lindqvist, J. K., Shepherd, C., Beu, A. G., Bannister, J. M., and Stein, J. K.: Subtropical rainforest vegetation from Cosy Dell, Southland: Plant fossil evidence for Late Oligocene terrestrial ecosystems, *N. Zeal. J. Geol. Geophys.*, 57, 236–252, <https://doi.org/10.1080/00288306.2014.888357>, 2014.
- Couvreur, T. L. P., Dauby, G., Blach-Overgaard, A., Deblauwe, V., Dessein, S., Droissart, V., Hardy, O. J., Harris, D. J., Janssens, S. B., Ley, A. C., Mackinder, B. A., Sonké, B., Sosef, M. S. M., Stévart, T., Svenning, J., Wieringa, J. J., Faye, A., Missoup, A. D., Tolley, K. A., Nicolas, V., Ntie, S., Fluteau, F., Robin, C., Guilloucheau, F., Barbini, D., and Sepulchre, P.: Tectonics, climate and the diversification of the tropical African terrestrial flora and fauna, *Biol. Rev.*, 96, 16–51, <https://doi.org/10.1111/brv.12644>, 2021.
- Cox, M. D.: An Idealized Model of the World Ocean. Part I: The Global-Scale Water Masses, *J. Phys. Oceanogr.*, 19, 1730–1752, 1989.
- Coxall, H. K. and Pearson, P. N.: The Eocene – Oligocene Transition, *Geol. Soc. Lond. Spec. Publ.*, 2, 351–387, 2007.
- Coxall, H. K. and Wilson, P. A.: Early Oligocene glaciation and productivity in the eastern equatorial Pacific: Insights into global carbon cycling, *Paleoceanography*, 26, 1–18, <https://doi.org/10.1029/2010PA002021>, 2011.
- Cramer, F., Magni, V., Domeier, M., Shephard, G. E., Chotalia, K., Cooper, G., Eakin, C. M., Grima, A. G., Gürer, D., Király, Á., Mulyukova, E., Peters, K., Robert, B., and Thielmann, M.: A transdisciplinary and community-driven database to unravel subduction zone initiation, *Nat. Commun.*, 11, 3750, <https://doi.org/10.1038/s41467-020-17522-9>, 2020.
- Cramwinckel, M., Burls, N. J., Fahad, A. A., Knapp, S., West, C. K., Reichgelt, T., Greenwood, D. R., Chan, W.-L., Donnadieu, Y., Hutchinson, D., De Boer, A. M., Ladant, J.-B., Morozova, P., Niezgodzki, I., Knorr, G., Steinig, S., Zhang, Z., Zhu, J., Feng, R., Lunt, D. J., Abe-Ouchi, A., and Inglis, G. N.: Global- and regional-scale hydrological response to early Eocene warmth, *ESS Open Archive*, <https://doi.org/10.1002/essoar.10512308.1>, 2022.
- Cramwinckel, M. J., Huber, M., Kocken, I. J., Agnini, C., Bijl, P. K., Bohaty, S. M., Frieling, J., Goldner, A., Hilgen, F. J., Kip, E. L., Peterse, F., van der Ploeg, R., Röhl, U., Schouten, S., and Sluijs, A.: Synchronous tropical and polar temperature evolution in the Eocene, *Nature*, 559, 382–386, <https://doi.org/10.1038/s41586-018-0272-2>, 2018.
- Creech, J. B., Baker, J. A., Hollis, C. J., Morgans, H. E. G., and Smith, E. G. C.: Eocene sea temperatures for the mid-latitude southwest Pacific from Mg/Ca ratios in planktonic and benthic foraminifera, *Earth Planet. Sc. Lett.*, 299, 483–495, <https://doi.org/10.1016/j.epsl.2010.09.039>, 2010.
- DeConto, R. M., Pollard, D., Wilson, P. A., Pälike, H., Lear, C. H., and Pagani, M.: Thresholds for Cenozoic bipolar glaciation, *Nature*, 455, 652–656, <https://doi.org/10.1038/nature07337>, 2008.
- De Man, E. and Simaeys, S. V.: Late Oligocene Warming Event in the southern North Sea Basin: benthic foraminifera as paleotemperature proxies, *Neth. J. Geosci.*, 83, 227–239, <https://doi.org/10.1017/S0016774600020291>, 2004.
- De Man, E., Van Simaeys, S., Vandenberghe, N., Harris, W. B., and Wampler, J. M.: On the nature and chronostratigraphic position of the Rupelian and Chattian stratotypes in the southern North Sea basin, *Episodes*, 33, 3–14, <https://doi.org/10.18814/epiugs/2010/v33i1/002>, 2010.
- De Vleeschouwer, D., Vahlenkamp, M., Crucifix, M., and Pälike, H.: Alternating Southern and Northern Hemisphere climate response to astronomical forcing during the past 35 m.y., *Geology*, 45, 375–378, <https://doi.org/10.1130/G38663.1>, 2017.
- DeConto, R. M. and Pollard, D.: Rapid Cenozoic glaciation of Antarctica induced by declining atmospheric CO₂, *Nature*, 421, 245–249, <https://doi.org/10.1038/nature01290>, 2003.

- Dielforder, A.: Constraining the strength of megathrusts from fault geometries and application to the Alpine collision zone, *Earth Planet. Sc. Lett.*, 474, 49–58, <https://doi.org/10.1016/j.epsl.2017.06.021>, 2017.
- Diester-Haass, L. and Zahn, R.: Eocene-Oligocene transition in the Southern Ocean: History of water mass circulation and biological productivity, *Geology*, 24, 163–166, 1996.
- Ding, L., Spicer, R. A., Yang, J., Xu, Q., Cai, F., Li, S., Lai, Q., Wang, H., Spicer, T. E. V., Yue, Y., Shukla, A., Srivastava, G., Khan, M. A., Bera, S., and Mehrotra, R.: Quantifying the rise of the Himalaya orogen and implications for the South Asian monsoon, *Geology*, 45, 215–218, <https://doi.org/10.1130/G38583.1>, 2017.
- Douglas, P. M. J., Affek, H. P., Ivany, L. C., Houben, A. J. P., Sijp, W. P., Sluijs, A., Schouten, S., and Pagani, M.: Pronounced zonal heterogeneity in Eocene southern high-latitude sea surface temperatures, *P. Natl. Acad. Sci. USA*, 111, 6582–6587, <https://doi.org/10.1073/pnas.1321441111>, 2014.
- Dumont, M. A.: Rapport sur la carte géologique du Royaume, Belgique de l'Académie royale des Sciences et des Lettres de la Belgique, 16, 351–373, 1849.
- Dupont-Nivet, G., Krijgsman, W., Langereis, C. G., Abels, H. A., Dai, S., and Fang, X.: Tibetan plateau aridification linked to global cooling at the Eocene–Oligocene transition, *Nature*, 445, 635–638, <https://doi.org/10.1038/nature05516>, 2007.
- Eagles, G.: Tectonic Reconstructions of the Southernmost Andes and the Scotia Sea During the Opening of the Drake Passage, in: *Geodynamic Evolution of the Southernmost Andes*, edited by: Ghiglione, C. M., Springer International Publishing, Cham, 75–108, https://doi.org/10.1007/978-3-319-39727-6_4, 2016.
- Eagles, G. and Jokat, W.: Tectonic reconstructions for paleobathymetry in Drake Passage, *Tectonophysics*, 611, 28–50, <https://doi.org/10.1016/j.tecto.2013.11.021>, 2014.
- Ehrmann, W. U. and Mackensen, A.: Sedimentological Evidence for the Formation of an East Antarctic Ice Sheet in Eocene/Oligocene Time, *Palaeogeogr. Palaeoclim. Palaeoecol.*, 93, 85–112, [https://doi.org/10.1016/0031-0182\(92\)90185-8](https://doi.org/10.1016/0031-0182(92)90185-8), 1992.
- Eldrett, J. S., Harding, I. C., Wilson, P. A., Butler, E., and Roberts, A. P.: Continental ice in Greenland during the Eocene and Oligocene, *Nature*, 446, 176–179, <https://doi.org/10.1038/nature05591>, 2007.
- Eldrett, J. S., Greenwood, D. R., Harding, I. C., and Huber, M.: Increased seasonality through the Eocene to Oligocene transition in northern high latitudes, *Nature*, 459, 969–973, <https://doi.org/10.1038/nature08069>, 2009.
- Erdei, B., Utescher, T., Hably, L., Tamás, J., Roth-Nebelsick, A., and Grein, M.: Early Oligocene Continental Climate of the Palaeogene Basin (Hungary and Slovenia) and the Surrounding Area, *Turk. J. Earth Sci.*, 21, 153–186, <https://doi.org/10.3906/yer-1005-29>, 2012.
- Evangelinos, D., Escutia, C., Etourneau, J., Hoem, F., Bijl, P., Boterblom, W., van de Flierdt, T., Valero, L., Flores, J.-A., Rodriguez-Tovar, F. J., Jimenez-Espejo, F. J., Salabarria, A., and López-Quirós, A.: Late Oligocene-Miocene proto-Antarctic Circumpolar Current dynamics off the Wilkes Land margin, East Antarctica, *Global Planet. Change*, 191, 103221, <https://doi.org/10.1016/j.gloplacha.2020.103221>, 2020.
- Evangelinos, D., Escutia, C., van de Flierdt, T., Valero, L., Flores, J.-A., Harwood, D. M., Hoem, F. S., Bijl, P., Etourneau, J., Kreis, sig, K., Nilsson-Kerr, K., Holder, L., López-Quirós, A., and Salabarnada, A.: Absence of a strong, deep-reaching Antarctic Circumpolar Current zonal flow across the Tasmanian gateway during the Oligocene to early Miocene, *Global Planet. Change*, 208, 103718, <https://doi.org/10.1016/j.gloplacha.2021.103718>, 2022.
- Evans, D., Sagoo, N., Renema, W., Cotton, L. J., Müller, W., Todd, J. A., Saraswati, P. K., Stassen, P., Ziegler, M., Pearson, P. N., Valdes, P. J., and Affek, H. P.: Eocene greenhouse climate revealed by coupled clumped isotope-Mg/Ca thermometry, *P. Natl. Acad. Sci. USA*, 115, 1174–1179, <https://doi.org/10.1073/pnas.1714744115>, 2018.
- Farnsworth, A., Lunt, D. J., O'Brien, C. L., Foster, G. L., Inglis, G. N., Markwick, P., Pancost, R. D., and Robinson, S. A.: Climate Sensitivity on Geological Timescales Controlled by Non-linear Feedbacks and Ocean Circulation, *Geophys. Res. Lett.*, 46, 9880–9889, <https://doi.org/10.1029/2019GL083574>, 2019.
- Fenero, R., Cotton, L., Molina, E., and Monechi, S.: Micropalaeontological evidence for the late Oligocene Oi-2b global glaciation event at the Zarabanda section, Spain, *Palaeogeogr. Palaeoclim. Palaeoecol.*, 369, 1–13, <https://doi.org/10.1016/j.palaeo.2012.08.020>, 2013.
- Ferguson, D. K., Lee, D. E., Bannister, J. M., Zetter, R., Jordan, G. J., Vavra, N., and Mildenhall, D. C.: The taphonomy of a remarkable leaf bed assemblage from the Late Oligocene–Early Miocene Gore Lignite Measures, southern New Zealand, *Int. J. Coal Geol.*, 83, 173–181, <https://doi.org/10.1016/j.coal.2009.07.009>, 2010.
- Fischer, H., Meissner, K. J., Mix, A. C., Abram, N. J., Auer, J., Brovkin, V., Capron, E., Colombaroli, D., Daniau, A. L., Dyez, K. A., Felis, T., Finkelstein, S. A., Jaccard, S. L., McClymont, E. L., Rovere, A., Sutter, J., Wolff, E. W., Affolter, S., Bakker, P., Ballesteros-Cánovas, J. A., Barbante, C., Caley, T., Carlson, A. E., Churakova, O., Cortese, G., Cumming, B. F., Davis, B. A. S., De Vernal, A., Emile-Geay, J., Fritz, S. C., Gierz, P., Gottschalk, J., Holloway, M. D., Joos, F., Kucera, M., Loutre, M. F., Lunt, D. J., Marcisz, K., Marlon, J. R., Martinez, P., Masson-Delmotte, V., Nehrbass-Ahles, C., Otto-Btiesner, B. L., Raible, C. C., Risebrobakken, B., Sánchez Goñi, M. F., Arrigo, J. S., Sarnthein, M., Sjolte, J., Stocker, T. F., Velasquez Alvarez, P. A., Tinner, W., Valdes, P. J., Vogel, H., Wanner, H., Yan, Q., Yu, Z., Ziegler, M., and Zhou, L.: Palaeoclimate constraints on the impact of 2 °C anthropogenic warming and beyond, *Nat. Geosci.*, 11, 474–485, <https://doi.org/10.1038/s41561-018-0146-0>, 2018.
- Flower, B. P., Zachos, J. C. C., and Paul, H.: Milankovitch-scale climate variability recorded near the Oligocene/Miocene boundary, *Proc. Ocean Drill. Program*, 154, 433–439, <https://doi.org/10.2973/odp.proc.sr.154.141.1997>, 1997.
- Fokkema, C. D., Agterhuis, T., Gerritsma, D., de Goeij, M., Liu, X., de Regt, P., Rice, A., Vennema, L., Agnini, C., Bijl, P. K., Frielings, J., Huber, M., Peterse, F., and Sluijs, A.: Polar Amplification of Orbital-Scale Climate Variability in the Early Eocene Greenhouse World, *Clim. Past*, 20, 1303–1325, <https://doi.org/10.5194/cp-20-1303-2024>, 2024.
- Fordyce, R. E.: Whale evolution and Oligocene southern ocean environments, *Palaeogeogr. Palaeoclim. Palaeoecol.*, 31, 319–336, [https://doi.org/10.1016/0031-0182\(80\)90024-3](https://doi.org/10.1016/0031-0182(80)90024-3), 1980.
- Foster, G. L., Royer, D. L., and Lunt, D. J.: Future climate forcing potentially without precedent in the last 420 million years, *Nat. Commun.*, 8, 1–8, <https://doi.org/10.1038/ncomms14845>, 2017.

- Fuchs, T.: Tertiärfossilien aus den kohlenführenden Miocaenablagerungen der Umgebung von Krapina und Radoboj und über die Stellung der sogenannten "Aquitaneische Stufe", Mitteilungen aus dem Jahrbuche der Kgl. Ungarischen Geologischen Anstalt, 10, 161–175, 1894.
- Galeotti, S., DeConto, R., Naish, T., Stocchi, P., Florindo, F., Paganini, M., Barrett, P., Bohaty, S. M., Lanci, L., Pollard, D., Sandroni, S., Talarico, F. M., and Zachos, J. C.: Antarctic Ice Sheet variability across the Eocene-Oligocene boundary climate transition, *Science*, 352, 76–80, 2016.
- Gaskell, D. E., Huber, M., O'Brien, C. L., Inglis, G. N., Acosta, R. P., Poulsen, C. J., and Hull, P. M.: The latitudinal temperature gradient and its climate dependence as inferred from foraminiferal $\delta^{18}\text{O}$ over the past 95 million years, *P. Natl. Acad. Sci. USA*, 119, e2111332119, <https://doi.org/10.1073/pnas.2111332119>, 2022.
- Gastaldo, R. A., Riegel, W., Püttmann, W., Linnemann, U. G., and Zetter, R.: A multidisciplinary approach to reconstruct the Late Oligocene vegetation in central Europe, *Rev. Palaeobot. Palynol.*, 101, 71–94, [https://doi.org/10.1016/S0034-6667\(97\)00070-5](https://doi.org/10.1016/S0034-6667(97)00070-5), 1998.
- Goldner, A., Herold, N., and Huber, M.: Antarctic glaciation caused ocean circulation changes at the Eocene-Oligocene transition, *Nature*, 511, 574–577, <https://doi.org/10.1038/nature13597>, 2014.
- Gradstein, F. M.: Introduction, in: *Geologic Time Scale 2020*, Elsevier, 3–20, <https://doi.org/10.1016/B978-0-12-824360-2.00001-2>, 2020.
- Greenop, R., Sosdian, S. M., Henehan, M. J., Wilson, P. A., Lear, C. H., and Foster, G. L.: Orbital Forcing, Ice Volume, and CO_2 Across the Oligocene-Miocene Transition, *Paleoceanogr. Paleoclim.*, 34, 316–328, <https://doi.org/10.1029/2018PA003420>, 2019.
- Gregory, K. M. and McIntosh, W. C.: Paleoclimate and paleoelevation of the Oligocene Pitch-Pinnacle flora, Sawatch Range, Colorado, *Geol. Soc. Am. Bull.*, 108, 545–561, [https://doi.org/10.1130/0016-7606\(1996\)108<0545:PAPOTO>2.3.CO;2](https://doi.org/10.1130/0016-7606(1996)108<0545:PAPOTO>2.3.CO;2), 1996.
- Gutián, J. and Stoll, H. M.: Evolution of Sea Surface Temperature in the Southern Mid-latitudes From Late Oligocene Through Early Miocene, *Paleoceanogr. Paleoclim.*, 36, 1–16, <https://doi.org/10.1029/2020PA004199>, 2021.
- Gutián, J., Phelps, S., Polissar, P. J., Ausín, B., Eglinton, T. I., and Stoll, H. M.: Midlatitude Temperature Variations in the Oligocene to Early Miocene, *Paleoceanogr. Paleoclim.*, 34, 1328–1343, <https://doi.org/10.1029/2019PA003638>, 2019.
- Hardenbol, J. and Berggren, W. A.: A New Paleogene Numerical Time Scale, *Am. Assoc. Petrol. Geol. Stud. Geol.*, 6, 213–234, 1978.
- Hartman, J. D., Sangiorgi, F., Salabarnada, A., Peterse, F., Houben, A. J. P., Schouten, S., Brinkhuis, H., Escutia, C., and Bijl, P. K.: Paleoceanography and ice sheet variability offshore Wilkes Land, Antarctica – Part 3: Insights from Oligocene-Miocene TEX₈₆-based sea surface temperature reconstructions, *Clim. Past*, 14, 1275–1297, <https://doi.org/10.5194/cp-14-1275-2018>, 2018.
- Heureux, A. M. C. and Rickaby, R. E. M.: Refining our estimate of atmospheric CO_2 across the Eocene–Oligocene climatic transition, *Earth Planet. Sc. Lett.*, 409, 329–338, <https://doi.org/10.1016/j.epsl.2014.10.036>, 2015.
- Hill, D. J., Haywood, A. M., Valdes, P. J., Francis, J. E., Lunt, D. J., Wade, B. S., and Bowman, V. C.: Paleogeographic controls on the onset of the Antarctic circumpolar current, *Geophys. Res. Lett.*, 40, 5199–5204, <https://doi.org/10.1002/grl.50941>, 2013.
- Ho, S. L. and Laepple, T.: Flat meridional temperature gradient in the early Eocene in the subsurface rather than surface ocean, *Nat. Geosci.*, 9, 606–610, <https://doi.org/10.1038/ngeo2763>, 2016.
- Hoem, F. S., Valero, L., Evangelinos, D., Escutia, C., Duncan, B., McKay, R. M., Brinkhuis, H., Sangiorgi, F., and Bijl, P. K.: Temperate Oligocene surface ocean conditions offshore of Cape Adare, Ross Sea, Antarctica, *Clim. Past*, 17, 1423–1442, <https://doi.org/10.5194/cp-17-1423-2021>, 2021.
- Hoem, F. S., Sauermilch, I., Aleksinski, A. K., Huber, M., Peterse, F., Sangiorgi, F., and Bijl, P. K.: Strength and variability of the Oligocene Southern Ocean surface temperature gradient, *Commun. Earth Environ.*, 3, 1–8, <https://doi.org/10.1038/s43247-022-00666-5>, 2022.
- Holland, M. M. and Bitz, C. M.: Polar amplification of climate change in coupled models, *Clim. Dynam.*, 21, 221–232, <https://doi.org/10.1007/s00382-003-0332-6>, 2003.
- Hollis, C. J., Dunkley Jones, T., Anagnostou, E., Bijl, P. K., Cramwinckel, M. J., Cui, Y., Dickens, G. R., Edgar, K. M., Eley, Y., Evans, D., Foster, G. L., Frieling, J., Inglis, G. N., Kennedy, E. M., Kozdon, R., Lauretano, V., Lear, C. H., Littler, K., Lourens, L., Meckler, A. N., Naafs, B. D. A., Pälike, H., Pancost, R. D., Pearson, P. N., Röhl, U., Royer, D. L., Salzmann, U., Schubert, B. A., Seebeck, H., Sluijs, A., Speijer, R. P., Stassen, P., Tierney, J., Tripati, A., Wade, B., Westerhold, T., Witkowski, C., Zachos, J. C., Zhang, Y. G., Huber, M., and Lunt, D. J.: The DeepMIP contribution to PMIP4: methodologies for selection, compilation and analysis of latest Paleocene and early Eocene climate proxy data, incorporating version 0.1 of the DeepMIP database, *Geosci. Model Dev.*, 12, 3149–3206, <https://doi.org/10.5194/gmd-12-3149-2019>, 2019.
- Houben, A. J. P., van Mourik, C. A., Montanari, A., Coccioni, R., and Brinkhuis, H.: The Eocene-Oligocene transition: Changes in sea level, temperature or both?, *Palaeogeogr. Palaeoclim. Palaeoecol.*, 335–336, 75–83, <https://doi.org/10.1016/j.palaeo.2011.04.008>, 2012.
- Houben, A. J. P., Bijl, P. K., Pross, J., Bohaty, S. M., Passchier, S., Stickley, C. E., Röhl, U., Sugisaki, S., Tauxe, L., van de Flierdt, T., Olney, M., Sangiorgi, F., Sluijs, A., Escutia, C., Brinkhuis, H., and the Expedition 318 Scientists: Reorganization of Southern Ocean Plankton Ecosystem at the Onset of Antarctic Glaciation, *Science*, 340, 341–344, <https://doi.org/10.1126/science.1223646>, 2013.
- Houben, A. J. P., Bijl, P. K., Sluijs, A., Schouten, S., and Brinkhuis, H.: Late Eocene Southern Ocean Cooling and Invigoration of Circulation Preconditioned Antarctica for Full-Scale Glaciation, *Geochem. Geophys. Geosy.*, 20, 2019GC008182, <https://doi.org/10.1029/2019GC008182>, 2019.
- Huang, B., Banzon, V. F., Freeman, E., Lawrimore, J., Liu, W., Peterson, T. C., Smith, T. M., Thorne, P. W., Woodruff, S. D., and Zhang, H.-M.: Extended Reconstructed Sea Surface Temperature Version 4 (ERSST.v4). Part I: Upgrades and Intercomparisons, *J. Climate*, 28, 911–930, <https://doi.org/10.1175/JCLI-D-14-00006.1>, 2015.

- Huber, M. and Caballero, R.: The early Eocene equitable climate problem revisited, *Clim. Past*, 7, 603–633, <https://doi.org/10.5194/cp-7-603-2011>, 2011.
- Huber, M., Brinkhuis, H., Stickley, C. E., Döös, K., Sluijs, A., Warnaar, J., Schellenberg, S. A., and Williams, G. L.: Eocene circulation of the Southern Ocean: Was Antarctica kept warm by subtropical waters?, *Paleoceanography*, 19, 1–12, <https://doi.org/10.1029/2004PA001014>, 2004.
- Hurley, S. J., Lipp, J. S., Close, H. G., Hinrichs, K.-U., and Pearson, A.: Distribution and export of isoprenoid tetraether lipids in suspended particulate matter from the water column of the Western Atlantic Ocean, *Org. Geochem.*, 116, 90–102, <https://doi.org/10.1016/j.orggeochem.2017.11.010>, 2018.
- Hutchinson, D. K., de Boer, A. M., Coxall, H. K., Caballero, R., Nilsson, J., and Baatsen, M.: Climate sensitivity and meridional overturning circulation in the late Eocene using GFDL CM2.1, *Clim. Past*, 14, 789–810, <https://doi.org/10.5194/cp-14-789-2018>, 2018.
- Hutchinson, D. K., Coxall, H. K., Lunt, D. J., Steinhorsdottir, M., de Boer, A. M., Baatsen, M., von der Heydt, A., Huber, M., Kennedy-Asser, A. T., Kunzmann, L., Ladant, J.-B., Lear, C. H., Morawec, K., Pearson, P. N., Piga, E., Pound, M. J., Salzmann, U., Scher, H. D., Sijp, W. P., Śliwińska, K. K., Wilson, P. A., and Zhang, Z.: The Eocene–Oligocene transition: a review of marine and terrestrial proxy data, models and model–data comparisons, *Clim. Past*, 17, 269–315, <https://doi.org/10.5194/cp-17-269-2021>, 2021.
- Inglis, G. N., Farnsworth, A., Lunt, D. J., Foster, G. L., Hollis, C. J., Paganí, M., Jardine, P. E., Pearson, P. N. P., Markwick, P., Galsworthy, A. M. J., Raynham, L., Taylor, K. W. R., and Pancost, R. D.: Descent toward the Icehouse: Eocene sea surface cooling inferred from GDGT distributions, *Paleoceanography*, 30, 1000–1020, <https://doi.org/10.1002/2014PA002723>, 2015.
- IPCC: Climate Change 2022: Impacts, Adaptation and Vulnerability, in: Contribution of Working Group II to the Sixth Assessment Report of the Intergovernmental Panel on Climate Change, 1st Edn., edited by: Pörtner, H.-O., Roberts, D. C., Tignor, M., Poloczanska, E. S., Mintenbeck, K., Alegría, A., Craig, M., Langsdorf, S., Löschke, S., Möller, V., Okem, A., and Rama, B., Cambridge University Press, Cambridge, 3056 pp., <https://doi.org/10.1017/9781009325844>, 2022.
- Jaramillo, C., Rueda, M. J., and Mora, G.: Cenozoic Plant Diversity in the Neotropics, *Science*, 311, 1893–1896, <https://doi.org/10.1126/science.1121380>, 2006.
- Jenny, D., Reichgelt, T., O'Brien, C., Liu, X., Bijl, P., Huber, M., and Sluijs, A.: Climate variability, heat distribution, and polar amplification in the warm unipolar “icehouse” of the Oligocene, Zenodo [code], <https://doi.org/10.5281/zenodo.10144091>, 2023b.
- Jenny, D., Reichgelt, T., O'Brien, C., Liu, X., Bijl, P., Huber, M., and Sluijs, A.: Climate variability, heat distribution, and polar amplification in the warm unipolar “icehouse” of the Oligocene [Data set], Zenodo [data set], <https://doi.org/10.5281/zenodo.10143889>, 2023b.
- Kast, E. R., Stolper, D. A., Auderset, A., Higgins, J. A., Ren, G. H., Wang, X., Martinez-Garcia, A., Haug, G. H., and Sigman, D. M.: Nitrogen isotope evidence for expanded ocean suboxia in the early Cenozoic, *Paleoceanography*, 364, 386–389, <https://doi.org/10.1126/science.aau5784>, 2019.
- Kvaček, Z., Hably, L., and Manchester, S. R.: Sloanea (Elaeocarpaceae) fruits and foliage from the Early Oligocene of Hungary and Slovenia, *Palaeontographica Abt. B*, 259, 113–124, <https://doi.org/10.1127/palb/259/2001/113>, 2001.
- Kennedy, A. T., Farnsworth, A., Lunt, D. J., Lear, C. H., and Markwick, P. J.: Atmospheric and oceanic impacts of Antarctic glaciation across the Eocene–Oligocene transition, *Philos. T. Roy. Soc. A*, 373, 1–18, <https://doi.org/10.1098/rsta.2014.0419>, 2015.
- Kennedy-Asser, A. T., Lunt, D. J., Farnsworth, A., and Valdes, P. J.: Assessing Mechanisms and Uncertainty in Modeled Climatic Change at the Eocene–Oligocene Transition, *Paleoceanogr. Paleoclim.*, 34, 16–34, <https://doi.org/10.1029/2018PA003380>, 2019.
- Kennett, J. P.: Cenozoic evolution of Antarctic glaciation, the circum-Antarctic Ocean, and their impact on global paleoceanography, *J. Geophys. Res.*, 82, 3843–3860, <https://doi.org/10.1029/jc082i027p03843>, 1977.
- Kim, J.-H., van der Meer, J., Schouten, S., Helmke, P., Willmott, V., Sangiorgi, F., Koç, N., Hopmans, E. C., and Damsté, J. S. S.: New indices and calibrations derived from the distribution of crenarchaeal isoprenoid tetraether lipids: Implications for past sea surface temperature reconstructions, *Geochim. Cosmochim. Ac.*, 74, 4639–4654, <https://doi.org/10.1016/j.gca.2010.05.027>, 2010.
- Kim, S.-T. and O'Neil, J. R.: Equilibrium and nonequilibrium oxygen isotope effects in synthetic carbonates, *Geochim. Cosmochim. Ac.*, 61, 3461–3475, [https://doi.org/10.1016/S0016-7037\(97\)00169-5](https://doi.org/10.1016/S0016-7037(97)00169-5), 1997.
- Köhler, P., de Boer, B., von der Heydt, A. S., Stap, L. B., and van de Wal, R. S. W.: On the state dependency of the equilibrium climate sensitivity during the last 5 million years, *Clim. Past*, 11, 1801–1823, <https://doi.org/10.5194/cp-11-1801-2015>, 2015.
- Kohn, M. J., Strömberg, C. A. E., Madden, R. H., Dunn, R. E., Evans, S., Palacios, A., and Carlini, A. A.: Quasi-static Eocene–Oligocene climate in Patagonia promotes slow faunal evolution and mid-Cenozoic global cooling, *Palaeogeogr. Palaeoclim. Palaeoeco.*, 435, 24–37, <https://doi.org/10.1016/j.palaeo.2015.05.028>, 2015.
- Kothoff, U., Greenwood, D. R., McCarthy, F. M. G., Müller-Navarra, K., Prader, S., and Hesselbo, S. P.: Late Eocene to middle Miocene (33 to 13 million years ago) vegetation and climate development on the North American Atlantic Coastal Plain (IODP Expedition 313, Site M0027), *Clim. Past*, 10, 1523–1539, <https://doi.org/10.5194/cp-10-1523-2014>, 2014.
- Kováč, M.: The Central Paratethys Palaeoceanography: A Water Circulation Model Based on Microfossil Proxies, Climate, and Changes of Depositional Environment, *Acta Geolog. Slovaca*, 9, 75–114, 2017.
- Kovar-Eder, J.: Early Oligocene plant diversity along the Upper Rhine Graben: The fossil flora of Rauenberg, Germany, *Acta Palaeobot.*, 56, 329–440, <https://doi.org/10.1515/acpa-2016-0011>, 2016.
- Kunzmann, L. and Walther, H.: Early Oligocene plant taphocoenoses of the Haselbach megafloral complex and the reconstruction of palaeovegetation, *Palaeobiol. Palaeoenviron.*, 92, 295–307, <https://doi.org/10.1007/s12549-012-0078-4>, 2012.
- Kvaček, Z. and Walther, H.: The Oligocene Volcanic Flora of Suleticé-Berand Near Ústí Nad Labem, North Bohemia – A review, *Acta Mus. Nat. Pragae*, 50, 25–54, 1995.

- Kvaček, Z., Teodоридис, В., Mach, K., Přikryl, T., and Dvořák, Z.: Tracing the Eocene-Oligocene transition: A case study from North Bohemia, *Bull. Geosci.*, 89, 1411, <https://doi.org/10.3140/bull.geosci.1411>, 2014.
- Kvaček, Z., Teodоридис, В., and Zajíčová, J.: Revision of the early Oligocene flora of Hrazený hill (formerly Pirskenberg) in Kněžecí near Šluknov, North Bohemia, *Acta Mus. Nat. Pragae Ser. B*, 71, 55–102, <https://doi.org/10.14446/AMNP.2015.55>, 2015.
- Ladant, J.-B., Donnadieu, Y., Lefebvre, V., and Dumas, C.: The respective role of atmospheric carbon dioxide and orbital parameters on ice sheet evolution at the Eocene-Oligocene transition: Ice sheet evolution at the EOT, *Paleoceanography*, 29, 810–823, <https://doi.org/10.1002/2013PA002593>, 2014.
- Laepple, T., Ziegler, E., Weitzel, N., Hébert, R., Ellerhoff, B., Schoch, P., Martrat, B., Bothe, O., Moreno-Chamarro, E., Chevalier, M., Herbert, A., and Rehfeld, K.: Regional but not global temperature variability underestimated by climate models at supradecadal timescales, *Nat. Geosci.*, 16, 958–966, <https://doi.org/10.1038/s41561-023-01299-9>, 2023.
- Lagabrielle, Y., Goddérus, Y., Donnadieu, Y., Malavieille, J., and Suarez, M.: The tectonic history of Drake Passage and its possible impacts on global climate, *Earth Planet. Sc. Lett.*, 279, 197–211, <https://doi.org/10.1016/j.epsl.2008.12.037>, 2009.
- Laskarev, V.: Sur les équivalens du sarmatiien supérieur en Serbie, in: *Receuil de travaux offert à M. Jovan Cvijić par ses amis et collaborateurs*, edited by: Vujević, P., Državna štamparija kraljevine srba, Belgrade, Imprimerie de l'État royaume des Serbes, Croates et Slovènes, 73–85, 1924.
- Levy, R. H., Meyers, S. R., Naish, T. R., Golledge, N. R., McKay, R. M., Crampton, J. S., DeConto, R. M., De Santis, L., Florindo, F., Gasson, E. G. W., Harwood, D. M., Luyendyk, B. P., Powell, R. D., Clowes, C., and Kulhanek, D. K.: Antarctic ice-sheet sensitivity to obliquity forcing enhanced through ocean connections, *Nat. Geosci.*, 12, 132–137, <https://doi.org/10.1038/s41561-018-0284-4>, 2019.
- Liebrand, D., Beddow, H. M., Lourens, L. J., Pálike, H., Raffi, I., Bohaty, S. M., Hilgen, F. J., Saes, M. J. M., Wilson, P. A., van Dijk, A. E., Hodell, D. A., Kroon, D., Huck, C. E., and Batenburg, S. J.: Cyclostratigraphy and eccentricity tuning of the early Oligocene through early Miocene (30.1–17.1 Ma): Cibicides mundulus stable oxygen and carbon isotope records from Walvis Ridge Site 1264, *Earth Planet. Sc. Lett.*, 450, 392–405, <https://doi.org/10.1016/j.epsl.2016.06.007>, 2016.
- Liebrand, D., De Bakker, A. T. M., Beddow, H. M., Wilson, P. A., Bohaty, S. M., Ruessink, G., Pálike, H., Batenburg, S. J., Hilgen, F. J., Hodell, D. A., Huck, C. E., Kroon, D., Raffi, I., Saes, M. J. M., Van Dijk, A. E., and Lourens, L. J.: Evolution of the early Antarctic ice ages, *P. Natl. Acad. Sci. USA*, 114, 3867–3872, <https://doi.org/10.1073/pnas.1615440114>, 2017.
- Liu, Z., Tuo, S., Zhao, Q., Cheng, X., and Huang, W.: Deep-water Earliest Oligocene Glacial Maximum (EOGM) in South Atlantic, *Chinese Sci. Bull.*, 49, 2190–2197, <https://doi.org/10.1360/04wd0228>, 2004.
- Liu, Z., Pagani, M., Zinniker, D., DeConto, R., Huber, M., Brinkhuis, H., Shah, S. R., Leckie, R. M., and Pearson, A.: Global Cooling During the Eocene-Oligocene Climate Transition, *Science*, 323, 1187–1190, <https://doi.org/10.1126/science.1166368>, 2009.
- Liu, Z., He, Y., Jiang, Y., Wang, H., Liu, W., Bohaty, S. M., and Wilson, P. A.: Transient temperature asymmetry between hemispheres in the Palaeogene Atlantic Ocean, *Nat. Geosci.*, 11, 656–660, <https://doi.org/10.1038/s41561-018-0182-9>, 2018.
- Lunt, D. J., Farnsworth, A., Loptson, C., Foster, G. L., Markwick, P., O'Brien, C. L., Pancost, R. D., Robinson, S. A., and Wrobel, N.: Palaeogeographic controls on climate and proxy interpretation, *Clim. Past*, 12, 1181–1198, <https://doi.org/10.5194/cp-12-1181-2016>, 2016.
- Lunt, D. J., Bragg, F., Chan, W.-L., Hutchinson, D. K., Ladant, J.-B., Morozova, P., Niezgodzki, I., Steinig, S., Zhang, Z., Zhu, J., Abe-Ouchi, A., Anagnostou, E., de Boer, A. M., Coxall, H. K., Donnadieu, Y., Foster, G., Inglis, G. N., Knorr, G., Langenbroek, P. M., Lear, C. H., Lohmann, G., Poulsen, C. J., Sepulchre, P., Tierney, J. E., Valdes, P. J., Volodin, E. M., Dunkley Jones, T., Hollis, C. J., Huber, M., and Otto-Btiesner, B. L.: DeepMIP: model intercomparison of early Eocene climatic optimum (EECO) large-scale climate features and comparison with proxy data, *Clim. Past*, 17, 203–227, <https://doi.org/10.5194/cp-17-203-2021>, 2021.
- Ma, X., Jiang, H., Cheng, J., and Xu, H.: Spatiotemporal evolution of Paleogene palynoflora in China and its implication for development of the extensional basins in East China, *Rev. Palaeobot. Palynol.*, 184, 24–35, <https://doi.org/10.1016/j.revpalbo.2012.07.013>, 2012.
- Macphail, M. K., Hill, R. S., Forsyth, S. M., and Wells, P. M.: A Late Oligocene-Early Miocene cool climate flora in Tasmania, *Alcheringa*, 15, 87–106, <https://doi.org/10.1080/03115519108619011>, 1991.
- Mai, D. H.: Contribution to the flora of the middle Oligocene Calau Beds in Brandenburg, Germany, *Rev. Palaeobot. Palynol.*, 101, 43–70, [https://doi.org/10.1016/S0034-6667\(97\)00069-9](https://doi.org/10.1016/S0034-6667(97)00069-9), 1998.
- Maldonado, A., Bohoyo, F., Galindo-Zaldívar, J., Hernández-Molina, F. J., Lobo, F. J., Lodolo, E., Martos, Y. M., Pérez, L. F., Schreider, A. A., and Somoza, L.: A model of oceanic development by ridge jumping: Opening of the Scotia Sea, *Global Planet. Change*, 123, 152–173, <https://doi.org/10.1016/j.gloplacha.2014.06.010>, 2014.
- Manchester, S. R., Herrera, F., Fourtanier, E., Barron, J., and Martínez, J.-N.: Oligocene Age of the Classic Belén Fruit and Seed Assemblage of North Coastal Peru based on Diatom Biostratigraphy, *J. Geol.*, 120, 467–476, <https://doi.org/10.1086/665797>, 2012.
- Masson-Delmotte, V., Schulz, M., Abe-Ouchi, A., Beer, J., Ganopolski, A., Fidel, J., Rouco, G., Jansen, E., Lambeck, K., Luterbacher, J., Naish, T., Ramesh, R., Rojas, M., Shao, X., Anchukaitis, K., Arblaster, J., Bartlein, P. J., Benito, G., Clark, P., Comiso, J. C., Crowley, T., Deckker, P. D., de Vernal, A., Delmonte, B., DiNezio, P., Dowsett, H. J., Edwards, R. L., Fischer, H., Fleitmann, D., Foster, G., Fröhlich, C., Hall, A., Hargreaves, J., Haywood, A., Hollis, C., Krinner, G., Landais, A., Li, C., Lunt, D., Mahowald, N., McGregor, S., Meehl, G., Mitrovica, J. X., Moberg, A., Mudelsee, M., Muhs, D. R., Mulitza, S., Müller, S., Overland, J., Parrenin, F., Pearson, P., Robock, A., Rohling, E., Salzmann, U., Savarino, J., Sedláček, J., Shindell, D., Smerdon, J., Solomina, O., Tarasov, P., Vinther, B., Waelbroeck, C., Wolf, D., Yokoyama, Y., Yoshimori, M., Zachos, J., Zwart, D., Gupta, A. K., Rahimzadeh, F., Raynaud, D., and Wanner, H.: Information from Paleoclimate Archives, in: *Climate Change 2013*:

- The Physical Science Basis, Contribution of Working Group I to the Fifth Assessment Report of the Intergovernmental Panel on Climate Change, Cambridge University Press, 383–464, <https://doi.org/10.1017/CBO9781107415324.013>, 2013.
- Matsuura, K. and Willmott, C. J.: Terrestrial Air Temperature: 1900–2017 Gridded Monthly Time Series, <https://climate.geog.udel.edu/> (last access: 17 July 2024), 2018.
- Meckler, A. N., Sexton, P. F., Piasecki, A. M., Leutert, T. J., Marquardt, J., Ziegler, M., Agterhuis, T., Lourens, L. J., Rae, J. W. B., Barnet, J., Tripati, A., and Bernasconi, S. M.: Cenozoic evolution of deep ocean temperature from clumped isotope thermometry, *Science*, 377, 86–90, <https://doi.org/10.1126/science.abk0604>, 2022.
- Meschede, M. and Warr, L. N.: The Geology of Germany: A Process-Oriented Approach, Springer International Publishing, Cham, <https://doi.org/10.1007/978-3-319-76102-2>, 2019.
- Miller, K. G., Feigenson, M. D., Kent, D. V., and Olsson, R. K.: Upper Eocene to Oligocene isotope ($^{87}\text{Sr}/^{86}\text{Sr}$, $\delta^{18}\text{O}$, $\delta^{13}\text{C}$) standard section, Deep Sea Drilling Project Site 522, Paleoceanography, 3, 223–233, <https://doi.org/10.1029/PA003i002p00223>, 1988.
- Miller, K. G., Wright, J. D., and Fairbanks, R. G.: Unlocking the Ice House: Oligocene-Miocene oxygen isotopes, eustasy, and margin erosion, *J. Geophys. Res.*, 96, 6829–6848, <https://doi.org/10.1029/90JB02015>, 1991.
- Morawec, K., Grein, M., Konrad, W., Kvaček, J., Kova-Eder, J., Neinhuis, C., Traiser, C., and Kunzmann, L.: Leaf traits of long-ranging Paleogene species and their relationship with depositional facies, climate and atmospheric CO₂ level, *Palaeontographica*, 298, 93–172, <https://doi.org/10.1127/palb/2019/0062>, 2019.
- Müller, P. J., Kirst, G., Ruhland, G., von Storch, I., and Rosell-Melé, A.: Calibration of the alkenone paleotemperature index U_{37'} based on core-tops from the eastern South Atlantic and the global ocean (60°N–60°S), *Geochim. Cosmochim. Ac.*, 62, 1757–1772, [https://doi.org/10.1016/S0016-7037\(98\)00097-0](https://doi.org/10.1016/S0016-7037(98)00097-0), 1998.
- Murphy, M. G. and Kennett, J. P.: Development of Latitudinal Thermal Gradients During the Oligocene: Oxygen Isotope Evidence from the Southwest Pacific, Initial Reports of the DeepSea Drilling Project 90, Ocean Drilling Program, 1347–1360, <https://doi.org/10.2973/dsdp.proc.90.1986>, 1986.
- Naish, T. R., Wolfe, K. J., Barrett, P. J., Wilson, G. S., Atkins, C., Bohaty, S. M., Bücker, C. J., Claps, M., Davey, F. J., Dunbar, G. B., Dunn, A. G., Fielding, C. R., Florindo, F., Hannah, M. J., Harwood, D. M., Henrys, S. A., Krissek, L. A., Lavelle, M., van der Meer, J., McIntosh, W. C., Niessen, F., Passchier, S., Powell, R. D., Roberts, A. P., Sagnotti, L., Scherer, R. P., Strong, C. P., Talarico, F., Verosub, K. L., Villa, G., Watkins, D. K., Webb, P.-N., and Wonik, T.: Orbitally induced oscillations in the East Antarctic ice sheet at the Oligocene/Miocene boundary, *Nature*, 413, 719–723, <https://doi.org/10.1038/35099534>, 2001.
- O'Brien, C. L., Robinson, S. A., Pancost, R. D., Sinninghe Damsté, J. S., Schouten, S., Lunt, D. J., Alsenz, H., Bornemann, A., Bottini, C., Brassell, S. C., Farnsworth, A., Forster, A., Huber, B. T., Inglis, G. N., Jenkyns, H. C., Linnert, C., Littler, K., Markwick, P., McAnena, A., Mutterlose, J., Naafs, B. D. A., Püttmann, W., Sluijs, A., van Helmond, N. A. G. M., Vellekoop, J., Wagner, T., and Wrobel, N. E.: Cretaceous sea-surface temperature evolution: Constraints from TEX₈₆ and planktonic foraminiferal oxygen isotopes, *Earth-Sci. Rev.*, 172, 224–247, <https://doi.org/10.1016/j.earscirev.2017.07.012>, 2017.
- O'Brien, C. L., Huber, M., Thomas, E., Pagani, M., Super, J. R., and Elder, L. E.: The enigma of Oligocene climate and global surface temperature evolution, *P. Natl. Acad. Sci. USA*, 117, 25302–25309, <https://doi.org/10.1073/pnas.2003914117>, 2020.
- Pagani, M., Zachos, J. C., Freeman, K. H., Tipple, B., and Bohaty, S.: Marked Decline in Atmospheric Carbon Dioxide Concentrations During the Paleogene, *Science*, 309, 600–603, <https://doi.org/10.1126/science.1110063>, 2005.
- Pagani, M., Huber, M., Liu, Z., Bohaty, S. M., Henderiks, J., Sijp, W., Krishnan, S., and DeConto, R. M.: The Role of Carbon Dioxide During the Onset of Antarctic Glaciation, *Science*, 334, 1261–1264, <https://doi.org/10.1126/science.1203909>, 2011.
- Palaeosens Project Members: Making sense of palaeoclimate sensitivity, *Nature*, 491, 683–691, <https://doi.org/10.1038/nature11574>, 2012.
- Palazzi, L. and Barreda, V.: Major vegetation trends in the Tertiary of Patagonia (Argentina): A qualitative paleoclimatic approach based on palynological evidence, *Flora: Morphology, Distribution, Funct. Ecol. Plants*, 202, 328–337, <https://doi.org/10.1016/j.flora.2006.07.006>, 2007.
- Palcu, D. V. and Krijgsman, W.: The dire straits of Paratethys: gateways to the anoxic giant of Eurasia, *Geological Society London Special Publications*, <https://doi.org/10.1144/SP523-2021-73>, 2023.
- Pälike, H., Frazier, J., and Zachos, J. C.: Extended orbitally forced palaeoclimatic records from the equatorial Atlantic Ceará Rise, *Quaternary Sci. Rev.*, 25, 3138–3149, <https://doi.org/10.1016/j.quascirev.2006.02.011>, 2006a.
- Pälike, H., Norris, R. D., Herrle, J. O., Wilson, P. A., Coxall, H. K., Lear, C. H., Shackleton, N. J., Tripati, A. K., and Wade, B. S.: The heartbeat of the Oligocene climate system, *Science*, 314, 1894–1898, <https://doi.org/10.1126/science.1133822>, 2006b.
- Pan, A. D.: The late Oligocene (28–27 Ma) Guang River Flora from the Northwestern Plateau of Ethiopia, unpublished D. Phil. Thesis, Southern Methodist University, 2007.
- Paull, R. and Hill, R. S.: Early oligocene Callitris and Fitzroya (Cupressaceae) from Tasmania, *Am. J. Bot.*, 97, 809–820, <https://doi.org/10.3732/ajb.0900374>, 2010.
- Pavlyutkin, B. I.: New species of thermophilic plants from the Early Oligocene flora of Kraskino (Primorski Region) as evidence of its subtropic type, *Paleontol. J.*, 45, 698–704, <https://doi.org/10.1134/S003103011106013X>, 2011.
- Pearson, P. N., Foster, G. L., and Wade, B. S.: Atmospheric carbon dioxide through the Eocene–Oligocene climate transition, *Nature*, 461, 1110–1113, <https://doi.org/10.1038/nature08447>, 2009.
- Petersen, S. V. and Schrag, D. P.: Antarctic ice growth before and after the Eocene–Oligocene transition: New estimates from clumped isotope paleothermometry, *Paleoceanography*, 30, 1305–1317, <https://doi.org/10.1002/2014PA002769>, 2015.
- Pierrehumbert, R. T., Brognez, H., and Roca, R.: On the Relative Humidity of the Atmosphere, in: *The Global Circulation of the Atmosphere*, 143–185, ISBN 9780691242392 2002.
- Plancq, J., Mattioli, E., Pittet, B., Simon, L., and Grossi, V.: Productivity and sea-surface temperature changes recorded during the late Eocene–early Oligocene at DSDP Site 511 (South

- Atlantic), *Palaeogeogr. Palaeoclim. Palaeoecol.*, 407, 34–44, <https://doi.org/10.1016/j.palaeo.2014.04.016>, 2014.
- Pole, M., Hill, R., Green, N., and Macphail, M.: The Oligocene Berwick Quarry Flora – Rainforest in a Drying Environment, *Aust. Systematic Bot.*, 6, 399–427, <https://doi.org/10.1071/SB9930399>, 1993.
- Popov, S. V., Sychevskaya, E. K., Akhmet'ev, M. A., Zaporozhets, N. I., and Golovina, L. A.: Stratigraphy of the Maikop Group and Pteropoda Beds in northern Azerbaijan, *Stratigr. Geol. Correl.*, 16, 664–677, <https://doi.org/10.1134/S0869593808060063>, 2008.
- Prahl, F. G. and Wakeham, S. G.: Calibration of unsaturation patterns in long-chain ketone compositions for palaeotemperature assessment, *Nature*, 330, 367–369, <https://doi.org/10.1038/330367a0>, 1987.
- Prebble, M., Sim, R., Finn, J., and Fink, D.: A Holocene Pollen and Diatom Record from Vanderlin Island, Gulf of Carpentaria, Lowland Tropical Australia, *Quatern. Res.*, 64, 357–371, <https://doi.org/10.1016/j.yqres.2005.08.005>, 2005.
- Rae, J. W. B., Zhang, Y. G., Liu, X., Foster, G. L., Stoll, H. M., and Whiteford, R. D. M.: Atmospheric CO₂ over the Past 66 Million Years from Marine Archives, *Annu. Rev. Earth Planet. Sci.*, 49, 609–641, <https://doi.org/10.1146/annurev-earth-082420-063026>, 2021.
- Raine, J. I. and Askin, R. A.: Terrestrial Palynology of Cape Roberts Project Drillhole CRP-3, Victoria Land Basin, Antarctica, *Terra Antartica*, 8, 389–400, 2001.
- Raymo, M. E. and Ruddiman, W. F.: Tectonic forcing of late Cenozoic climate, *Nature*, 359, 117–122, <https://doi.org/10.1038/359117a0>, 1992.
- Reichgelt, T., Baumgartner, A., Feng, R., and Willard, D. A.: Poleward amplification, seasonal rainfall and forest heterogeneity in the Miocene of the eastern USA, *Global Planet. Change*, 222, 104073, <https://doi.org/10.1016/j.gloplacha.2023.104073>, 2023.
- Rögl, V. F.: Palaeogeographic Considerations for Mediterranean and Paratethys Seaways (Oligocene to Miocene), *Annalen des Naturhistorischen Museums in Wien*, 99, 279–310, 1998.
- Roth-Nebelsick, A., Oehm, C., Grein, M., Uttescher, T., Kunzmann, L., Friedrich, J.-P., and Konrad, W.: Stomatal density and index data of *Platanus neptuni* leaf fossils and their evaluation as a CO₂ proxy for the Oligocene, *Rev. Palaeobot. Palynol.*, 206, 1–9, <https://doi.org/10.1016/j.revpalbo.2014.03.001>, 2014.
- Salamy, K. A. and Zachos, J. C.: Latest Eocene-Early Oligocene climate change and Southern Ocean fertility: Inferences from sediment accumulation and stable isotope data, *Palaeogeogr. Palaeoclim. Palaeoecol.*, 145, 61–77, [https://doi.org/10.1016/S0031-0182\(98\)00093-5](https://doi.org/10.1016/S0031-0182(98)00093-5), 1999.
- Salard-Cheboldaeff, M.: Palynologie maestrichtienne et tertiaire du cameroun. Etude qualitative et repartition verticale des principales espèces, *Rev. Palaeobot. Palynol.*, 28, 365–388, [https://doi.org/10.1016/0034-6667\(79\)90032-0](https://doi.org/10.1016/0034-6667(79)90032-0), 1979.
- Sangiorgi, F., Bijl, P. K., Passchier, S., Salzmann, U., Schouten, S., McKay, R., Cody, R. D., Pross, J., van de Flierdt, T., Bohaty, S. M., Levy, R., Williams, T., Escutia, C., and Brinkhuis, H.: Southern Ocean warming and Wilkes Land ice sheet retreat during the mid-Miocene, *Nat. Commun.*, 9, 317, <https://doi.org/10.1038/s41467-017-02609-7>, 2018.
- Sauermilch, I., Whittaker, J. M., Klocker, A., Munday, D. R., Hochmuth, K., Bijl, P. K., and LaCasce, J. H.: Gateway-driven weakening of ocean gyres leads to Southern Ocean cooling, *Nat. Commun.*, 12, 6465, <https://doi.org/10.1038/s41467-021-26658-1>, 2021.
- Scher, H. D. and Martin, E. E.: Timing and Climatic Consequences of the Opening of Drake Passage, *Science*, 312, 428–430, <https://doi.org/10.1126/science.1120044>, 2006.
- Scher, H. D. and Martin, E. E.: Oligocene deep water export from the North Atlantic and the development of the Antarctic Circumpolar Current examined with neodymium isotopes, *Paleoceanography*, 23, 1–12, <https://doi.org/10.1029/2006PA001400>, 2008.
- Scher, H. D., Whittaker, J. M., Williams, S. E., Latimer, J. C., Kordes, W. E. C., and Delaney, M. L.: Onset of Antarctic Circumpolar Current 30 million years ago as Tasmanian Gateway aligned with westerlies, *Nature*, 523, 580–583, <https://doi.org/10.1038/nature14598>, 2015.
- Schouten, S., Hopmans, E. C., Schefuß, E., and Sinninghe Damsté, J. S.: Distributional variations in marine crenarchaeotal membrane lipids: a new tool for reconstructing ancient sea water temperatures?, *Earth Planet. Sc. Lett.*, 204, 265–274, [https://doi.org/10.1016/S0012-821X\(02\)00979-2](https://doi.org/10.1016/S0012-821X(02)00979-2), 2002.
- Schulz, H., Bechtel, A., and Sachsenhofer, R.: The birth of the Paratethys during the Early Oligocene: From Tethys to an ancient Black Sea analogue?, *Global Planet. Change*, 49, 163–176, <https://doi.org/10.1016/j.gloplacha.2005.07.001>, 2005.
- Scotese, C. and Wright, N. M.: PaleoDEM Resource, EarthByte, <https://www.earthbyte.org/paleodem-resource-scotese-and-wright-2018/> (last access: 17 July 2024), 2018.
- Shackleton, N. J.: Attainment of Isotopic Equilibrium Between Ocean Water and the Benthic Foraminifera genus *Uvigerina*: Isotopic Changes in the Ocean During the Last Glacial, *Colloques Internationaux du C.N.R.S.*, 219, 203–209, 1974.
- Silva, I. P. and Jenkins, D. G.: Decision on the Eocene-Oligocene boundary stratotype, *Episodes*, 16, 379–382, <https://doi.org/10.18814/epiugs/1993/v16i3/002>, 1993.
- Śliwińska, K. K., Clausen, O. R., and Heilmann-Clausen, C.: A mid-Oligocene cooling (O1-2b) reflected in the dinoflagellate record and in depositional sequence architecture. An integrated study from the eastern North Sea Basin, *Mar. Petrol. Geol.*, 27, 1424–1430, <https://doi.org/10.1016/j.marpetgeo.2010.03.008>, 2010.
- Sluiter, I. R. K., Holdgate, G. R., Reichgelt, T., Greenwood, D. R., Kershaw, A. P., and Schultz, N. L.: A new perspective on Late Eocene and Oligocene vegetation and paleoclimates of South-eastern Australia, *Palaeogeogr. Palaeoclim. Palaeoecol.*, 596, 110985, <https://doi.org/10.1016/j.palaeo.2022.110985>, 2022.
- Solé, F., Fischer, V., Denayer, J., Speijer, R. P., Fournier, M., Le Verger, K., Ladevèze, S., Folie, A., and Smith, T.: The upper Eocene-Oligocene carnivorous mammals from the Quercy Phosphorites (France) housed in Belgian collections, *Geol. Belg.*, 24, 1–16, <https://doi.org/10.20341/gb.2020.006>, 2020.
- Spero, H. J. and Williams, D. F.: Extracting environmental information from planktonic foraminiferal $\delta^{13}\text{C}$ data, *Nature*, 335, 717–719, <https://doi.org/10.1038/335717a0>, 1988.
- Spero, H. J., Bijma, J., Lea, D. W., and Bemis, B. E.: Effect of seawater carbonate concentration on foraminiferal carbon and oxygen isotopes, *Nature*, 390, 497–500, <https://doi.org/10.1038/37333>, 1997.

- Spicer, R. A., Farnsworth, A., and Su, T.: Cenozoic topography, monsoons and biodiversity conservation within the Tibetan Region: An evolving story, *Plant Divers.*, 42, 229–254, <https://doi.org/10.1016/j.pld.2020.06.011>, 2020.
- Spicer, R. A., Su, T., Valdes, P. J., Farnsworth, A., Wu, F.-X., Shi, G., Spicer, T. E. V., and Zhou, Z.: The topographic evolution of the Tibetan Region as revealed by palaeontology, *Palaeobiol. Palaeoenviron.*, 101, 213–243, <https://doi.org/10.1007/s12549-020-00452-1>, 2021a.
- Spicer, R. A., Su, T., Valdes, P. J., Farnsworth, A., Wu, F.-X., Shi, G., Spicer, T. E. V., and Zhou, Z.: Why ‘the uplift of the Tibetan Plateau’ is a myth, *Natl. Sci. Rev.*, 8, nwaa091, <https://doi.org/10.1093/nsr/nwaa091>, 2021b.
- Steininger, F. F. and Wessely, G.: From the Tethyan Ocean to the Paratethys Sea: Oligocene to Neogene Stratigraphy, Paleogeography and Paleobiogeography of the circum-Mediterranean region and the Oligocene to Neogene Basin evolution in Austria, *Mitt. Österr. Geol. Ges.*, 92, 95–116, 1999.
- Steininger, F. F., Aubry, M. P., Berggren, W. A., Biolzi, M., M. Borsetti, A., Cartlidge, J. E., Cati, F., Corfield, R., Gelati, R., Iaccarino, S., Napoleone, C., Ottner, F., Rögl, F., Roetzel, R., Spezzaferri, S., Tateo, F., Villa, G., and Zevenboom, D.: The Global Stratotype Section and Point (GSSP) for the base of the Neogene, *Episodes*, 20, 23–28, <https://doi.org/10.18814/epiugi/1997/v20i1/005>, 1997.
- Steinthorsdottir, M., Coxall, H. K., De Boer, A. M., Huber, M., Barbolini, N., Bradshaw, C. D., Burls, N. J., Feakins, S. J., Gasson, E., Henderiks, J., Holbourn, A. E., Kiel, S., Kohn, M. J., Knorr, G., Kürschner, W. M., Lear, C. H., Liebrand, D., Lunt, D. J., Mörs, T., Pearson, P. N., Pound, M. J., Stoll, H., and Strömberg, C. A. E.: The Miocene: The Future of the Past, *Paleoceanogr. Paleoclim.*, 36, 1–71, <https://doi.org/10.1029/2020PA004037>, 2021.
- Stickley, C. E., Brinkhuis, H., Schellenberg, S. A., Sluijs, A., Röhl, U., Fuller, M., Grauert, M., Huber, M., Warnaar, J., and Williams, G. L.: Timing and nature of the deepening of the Tasmanian Gateway: Deepening Of The Tasmanian Gateway, *Paleoceanography*, 19, 1–18, <https://doi.org/10.1029/2004PA001022>, 2004.
- Stickley, C. E., St John, K., Koç, N., Jordan, R. W., Passchier, S., Pearce, R. B., and Kearns, L. E.: Evidence for middle Eocene Arctic sea ice from diatoms and ice-rafted debris, *Nature*, 460, 376–379, <https://doi.org/10.1038/nature08163>, 2009.
- St. John, K.: Cenozoic ice-rafting history of the central Arctic Ocean: Terrigenous sands on the Lomonosov Ridge, *Paleoceanography*, 23, 1–12, <https://doi.org/10.1029/2007PA001483>, 2008.
- Su, T., Spicer, R. A., Li, S.-H., Xu, H., Huang, J., Sherlock, S., Huang, Y.-J., Li, S.-F., Wang, L., Jia, L.-B., Deng, W.-Y.-D., Liu, J., Deng, C.-L., Zhang, S.-T., Valdes, P. J., and Zhou, Z.-K.: Uplift, climate and biotic changes at the Eocene–Oligocene transition in south-eastern Tibet, *Natl. Sci. Rev.*, 6, 495–504, <https://doi.org/10.1093/nsr/nwy062>, 2019.
- Sun, J., Ni, X., Bi, S., Wu, W., Ye, J., Meng, J., and Windley, B. F.: Synchronous turnover of flora, fauna and climate at the Eocene–Oligocene Boundary in Asia, *Sci. Rep.*, 4, 1–6, <https://doi.org/10.1038/srep07463>, 2014.
- Super, J. R., Thomas, E., Pagani, M., Huber, M., O’Brien, C. L., and Hull, P. M.: Miocene Evolution of North Atlantic Sea Surface Temperature, *Paleoceanogr. Paleoclim.*, 35, 1–15, <https://doi.org/10.1029/2019PA003748>, 2020.
- Thompson, N., Salzmann, U., López-Quiros, A., Bijl, P. K., Hoem, F. S., Etourneau, J., Sicre, M.-A., Roignant, S., Hocking, E., Amoo, M., and Escutia, C.: Vegetation change across the Drake Passage region linked to late Eocene cooling and glacial disturbance after the Eocene–Oligocene transition, *Clim. Past*, 18, 209–232, <https://doi.org/10.5194/cp-18-209-2022>, 2022.
- Tierney, J. E. and Tingley, M. P.: A Bayesian, spatially-varying calibration model for the TEX₈₆ proxy, *Geochim. Cosmochim. Ac.*, 127, 83–106, <https://doi.org/10.1016/j.gca.2013.11.026>, 2014.
- Tierney, J. E. and Tingley, M. P.: BAYSPLINE: A New Calibration for the Alkenone Paleothermometer, *Paleoceanogr. Paleoclim.*, 33, 281–301, <https://doi.org/10.1002/2017PA003201>, 2018.
- Toggweiler, J. R. and Bjornsson, H.: Drake Passage and palaeoclimate, *J. Quaternary Sci.*, 15, 319–328, [https://doi.org/10.1002/1099-1417\(200005\)15:4<319::AID-JQS545>3.0.CO;2-C](https://doi.org/10.1002/1099-1417(200005)15:4<319::AID-JQS545>3.0.CO;2-C), 2000.
- Tosal, A. and Martín-Closas, C.: Taphonomy and palaeoecology of the Oligocene flora from Cervera (Catalonia, Spain) and their implication in palaeoclimatic reconstruction, *Rev. Palaeobot. Palynol.*, 233, 93–103, <https://doi.org/10.1016/j.revpalbo.2016.06.008>, 2016.
- Toumoulin, A., Donnadieu, Y., Ladant, J. -B., Batenburg, S. J., Poblete, F., and Dupont-Nivet, G.: Quantifying the Effect of the Drake Passage Opening on the Eocene Ocean, *Paleoceanogr. Paleoclim.*, 35, 1–22, <https://doi.org/10.1029/2020PA003889>, 2020.
- Tremblin, M., Hermoso, M., and Minoletti, F.: Equatorial heat accumulation as a long-term trigger of permanent Antarctic ice sheets during the Cenozoic, *P. Natl. Acad. Sci. USA*, 113, 11782–11787, <https://doi.org/10.1073/pnas.1608100113>, 2016.
- Tripathi, A., Backman, J., Elderfield, H., and Ferretti, P.: Eocene bipolar glaciation associated with global carbon cycle changes, *Nature*, 436, 341–346, <https://doi.org/10.1038/nature03874>, 2005.
- van de Lagemaat, S. H. A., Swart, M. L. A., Vaes, B., Kosters, M. E., Boschman, L. M., Burton-Johnson, A., Bijl, P. K., Spakman, W., and van Hinsbergen, D. J. J.: Subduction initiation in the Scotia Sea region and opening of the Drake Passage: When and why?, *Earth-Sci. Rev.*, 215, 103551, <https://doi.org/10.1016/j.earscirev.2021.103551>, 2021.
- van der Weijst, C. M. H., van der Laan, K. J., Peterse, F., Reichart, G.-J., Sangiorgi, F., Schouten, S., Veenstra, T. J. T., and Sluijs, A.: A 15-million-year surface- and subsurface-integrated TEX₈₆ temperature record from the eastern equatorial Atlantic, *Clim. Past*, 18, 1947–1962, <https://doi.org/10.5194/cp-18-1947-2022>, 2022.
- van Hinsbergen, D. J. J.: Indian plate paleogeography, subduction and horizontal underthrusting below Tibet: paradoxes, controversies and opportunities, *Natl. Sci. Rev.*, 9, nwac074, <https://doi.org/10.1093/nsr/nwac074>, 2022.
- Van Simaeys, S.: The Rupelian-Chattian boundary in the North Sea Basin and its calibration to the international time-scale, *Neth. J. Geosci.*, 83, 241–248, <https://doi.org/10.1017/S0016774600020308>, 2004.
- Van Simaeys, S., Man, E. D., Vandenberghe, N., Brinkhuis, H., and Steurbaut, E.: Stratigraphic and palaeoenvironmental analysis of the Rupelian-Chattian transition in the type region: Ev-

- idence from dinoflagellate cysts, foraminifera and calcareous nannofossils, *Palaeogeogr. Palaeoclim. Palaeoecol.*, 208, 31–58, <https://doi.org/10.1016/j.palaeo.2004.02.029>, 2004.
- Via, R. K. and Thomas, D. J.: Evolution of Atlantic thermohaline circulation: Early Oligocene onset of deep-water production in the North Atlantic, *Geology*, 34, 441–444, <https://doi.org/10.1130/G22545.1>, 2006.
- Wang, C., Dai, J., Zhao, X., Li, Y., Graham, S. A., He, D., Ran, B., and Meng, J.: Outward-growth of the Tibetan Plateau during the Cenozoic: A review, *Tectonophysics*, 621, 1–43, <https://doi.org/10.1016/j.tecto.2014.01.036>, 2014.
- Westerhold, T., Marwan, N., Drury, A. J., Liebrand, D., Agnini, C., Anagnostou, E., Barnet, J. S. K., Bohaty, S. M., De Vleeschouwer, D., Florindo, F., Frederichs, T., Hodell, D. A., Holbourn, A. E., Kroon, D., Lauretano, V., Littler, K., Lourens, L. J., Lyle, M., Pälike, H., Röhl, U., Tian, J., Wilkens, R. H., Wilson, P. A., and Zachos, J. C.: An astronomically dated record of Earth's climate and its predictability over the last 66 million years, *Science*, 369, 1383–1387, <https://doi.org/10.1126/science.aba6853>, 2020.
- Willard, D. A., Donders, T. H., Reichgelt, T., Greenwood, D. R., Sangiorgi, F., Peterse, F., Nierop, K. G. J., Frielink, J., Schouten, S., and Sluijs, A.: Arctic vegetation, temperature, and hydrology during Early Eocene transient global warming events, *Global Planet. Change*, 178, 139–152, <https://doi.org/10.1016/j.gloplacha.2019.04.012>, 2019.
- Winterberg, S., Picotti, V., and Willett, S. D.: Messinian or Pleistocene valley incision within the Southern Alps, *Swiss J. Geosci.*, 113, 7, <https://doi.org/10.1186/s00015-020-00361-7>, 2020.
- Witkowski, C. R., Weijers, J. W. H., Blais, B., Schouten, S., and Sinninghe Damsté, J. S.: Molecular fossils from phytoplankton reveal secular PCO_2 trend over the Phanerozoic, *Sci. Adv.*, 4, 1–8, <https://doi.org/10.1126/sciadv.aat4556>, 2018.
- Wright, N. M., Scher, H. D., Seton, M., Huck, C. E., and Duggan, B. D.: No Change in Southern Ocean Circulation in the Indian Ocean From the Eocene Through Late Oligocene, *Paleoceanogr. Paleoceanogr.*, 33, 152–167, <https://doi.org/10.1002/2017PA003238>, 2018.
- Wuchter, C., Schouten, S., Coolen, M. J. L., and Sinninghe Damsté, J. S.: Temperature-dependent variation in the distribution of tetraether membrane lipids of marine Crenarchaeota: Implications for TEX₈₆ paleothermometry, *Paleoceanography*, 19, 1–10, <https://doi.org/10.1029/2004PA001041>, 2004.
- Zachos, J. C., Quinn, T. M., and Salamy, K. A.: High-resolution deep-sea foraminiferal stable isotope records of the Eocene–Oligocene transition, *Paleoceanography*, 11, 251–266, 1996.
- Zanazzi, A., Kohn, M. J., MacFadden, B. J., and Terry, D. O.: Large temperature drop across the Eocene–Oligocene transition in central North America, *Nature*, 445, 639–642, <https://doi.org/10.1038/nature05551>, 2007.
- Zeebe, R. E., Bijma, J., and Wolf-Gladrow, D. A.: A diffusion-reaction model of carbon isotope fractionation in foraminifera, *Mar. Chem.*, 64, 199–227, [https://doi.org/10.1016/S0304-4203\(98\)00075-9](https://doi.org/10.1016/S0304-4203(98)00075-9), 1999.
- Zhang, Y. G., Pagani, M., Liu, Z., Bohaty, S. M., and DeConto, R.: A 40-million-year history of atmospheric CO_2 , *Philos. T. Roy. Soc. A*, 371, 20130096, <https://doi.org/10.1098/rsta.2013.0096>, 2013.